UNIVERSITAT POLITÈCNICA DE VALÈNCIA
&
UNIVERSITÀ DEGLI STUDI DI PADOVA

ESCOLA TÈCNICA SUPERIOR D'ENGINYERIA AGRONÒMICA I DEL MEDI NATURAL
&
DIPARTIMENTO DI SCIENZE DEL FARMACO

Bachelor's Degree in Biotechnology

Role of the N-terminal Methionine in the biophysical properties of α-synuclein

Author: Diego Ruiz Espi

Tutors:
Prof. Patrizia Polverino de Laureto
Prof. Lynne Yenush

Supervisors:
Benedetta Fongaro
Valentina Cian

València, June 2021

Abstract

Role of the N-terminal Methionine in the biophysical properties of α-synuclein

PD is a multifactorial pathology characterized by both motor and non-motor features; its development seems to be mainly linked to the formation of αSyn aggregates and their accumulation in dopaminergic neurons. αSyn is known to acquire an α-helical structure when interacting with biological membranes: the role of the four Met residues of αSyn in this type of interaction has not yet been investigated. Therefore, this study focuses on the analysis of the oxidized Met residues and the processing of the N-terminal one, as models to understand their role. Both αSyn and αSynOx are produced following procedures set up in the laboratory where the thesis work was performed. The production protocol for N-1-αSyn was not found in literature, therefore, several experiments are carried out to set-up the method. The best reaction conditions are yet found to have a very low yield. Due to the unfolding nature of αSyn, it is easier for the protease to cleave the entire polypeptide chain than to remove the first residue, therefore, it is complex to find an equilibrium where the protease cleaves the first residue without losing its specificity. Different sets of experiments are performed, firstly to characterize the three proteins from a chemical and conformational point of view; following, proteins were studied in the presence of two different membrane-mimetic systems: SDS and liposomes. The three proteins show α-helical structures upon encounter of the negatively charged surface in the presence of SDS and liposomes. Nevertheless, significant variations demonstrate that the N-terminal Met is not crucial for the anchoring of αSyn to the membrane, rejecting the last hypothesis on the field. These results are a starting point for further investigations related to the anchoring of αSyn to the cell membrane, crucial step in the PD pathogenesis.

Key words: α-synuclein; Methionine AminoPeptidase; N-terminal Methionine; membrane interaction; protein aggregation; amylogenic proteins.

Author: Diego Ruiz Espi

Tutors:
Prof. Patrizia Polverino de Laureto
Prof. Lynne Yenush

Supervisors:
Benedetta Fongaro
Valentina Cian

València, June 2021

Importància de la Metionina N-terminal en les propietats biofísiques de l'α-sinucleina.

PD és una patologia multifactorial caracteritzada tant per desordres motors com per altres no motors; el seu desenvolupament sembla estar principalment lligat a la formació d'agregats d'αSyn i la seua acumulació en les neurones dopaminèrgiques. αSyn adquireix estructura α-hèlice quan interacciona amb membranes biològiques: la importància dels quatre residus de metionina de la αSyn en aquest tipus d'interacció encara no ha estat investigada. És per això que aquest estudi es centra en l'anàlisi de l'oxidació dels residus de metionina i del processament de la metionina N-terminal, com a models per a entendre la seua importància. Tant l'αSyn com l'αSynOx es produeixen seguint els protocols establerts al laboratori on es va dur a terme el treball. El protocol de producció de la N-1-αSyn no es troba a la bibliografia, per la qual cosa es dissenyen diversos experiments per a determinar el millor mètode de producció. Fins i tot amb les condicions òptimes de producció, el rendiment de la reacció és molt baix. Açò es deu a que l'αSyn presenta una estructura de naturalesa desordenada que fa que la proteasa tinga més facilitat per tallar el polipèptid sencer que per fer-ho específicament amb la primera metionina. Per això, és complicat trobar un equilibri en el que la proteasa talla la metionina N-terminal sense perdre la especificitat. Diversos tipus d'experiments es duen a terme, primer per a caracteritzar les tres proteïnes des d'un punt de vista químic i conformacional; seguit d'un estudi en presència de dos tipus diferents de models de membrana biològica: micel·les de SDS i liposomes. Les tres proteïnes mostren una estructura α-hèlice quan interactuen amb superfícies carregades negativament en la presència de SDS o liposomes. No obstant això, variacions significatives demostren que la metionina N-terminal no és crucial per a l'àncora de la αSyn a la membrana, rebutjant l'última hipòtesi establerta en aquest camp. Aquests resultats són el punt d'inici per a futures investigacions relacionades amb l'àncora de l'αSyn a la membrana cel·lular, pas fonamental en la patogènesis del PD.

Paraules clau: α-sinucleina; Metionina-AminoPeptidasa; Metionina N-terminal; interacció de membrana; agregació proteica; proteïnes amilogèniques.

Autor: Diego Ruiz Espi

Tutores:
Prof. Patrizia Polverino de Laureto
Prof. Lynne Yenush

Supervisores:
Benedetta Fongaro
Valentina Cian

València, juny 2021

Contents

List of abbreviations

αSyn	α-Synuclein
αSynOx	Oxidized α-Synuclein
AD	Alzheimer's disease
CD	Circular dichroism
CMC	Critical micellar concentration
DA	Dopamine
DLS	Dynamic light scattering
EcMAP	Methionine aminopeptidase from *E.coli*
ESI	Electron-spray ionization
FPLC	Fast performance liquid chromatography
HPLC	High performance liquid chromatography
IEX	Ion-exchange chromatography
IDR	Intrinsically disordered protein regions
ITP	Integral Transmembrane Proteins
LBs	Lewy bodies
LC	Liquid chromatography
LNs	Lewy neurities
m/m	Mass-to-mass ratio
m/z	Mass to charge ratio
MLV	Multilamellar vesicles
MS	Mass spectrometry
MW	Molecular weight
N-1-αSyn	N-1-α-Synuclein
NAC	Amyloid-binding central domain
NaP	Sodium phosphate
o/n	overnight
PC	Phosphatidylcholine
PD	Parkinson's disease
PfMAP	Methionine aminopeptidase from *Pyrococcus furiosus*
PL	Phospholipid
PMP	Peripheral Membrane Proteins
PS	L-alpha-phosphatidylserine
Q	Quadrupole
RP-HPLC	Reverse phase - high performance liquid
SEC	Size-exclusion chromatography
SN	Substantia nigra
SUVs	Small unilamellar vesicles
TOF	Time-of-flight
ULVs	Unilamellar vesicles
WT	Wild type

1. Introduction

1.1. Parkinson's disease

Parkinson's disease (PD) is a chronic, progressive neurodegenerative disease that leads to both motor and non-motor dysfunctions. Its symptoms were first remarkably described by Dr. James Parkinson in 1817 as tremors, differentiating those "produced by attempts at voluntary motion versus those which occur whilst the body is at rest" [Obeso *et al*., 2017]. The motor dysfunctions are attributed to the loss of dopaminergic neurons and the non-motor dysfunctions are related with neuronal loss in non-dopaminergic areas. The pathophysiological changes start before the motor symptoms and normally include a number of non-motor presentations, such as sleep disturbance, depression, anxiety, dysautonomia and cognitive decline [DeMaagd & Philip, 2015]. In this moment, the patient is normally not aware because these first symptoms may be related with many other diseases or even with a stressful moment of life. Motor symptoms gradually come later, normally starting with the characteristic tremor in a hand and a feeling of stiffness in the body. Over time, bradykinesia and muscular rigidity may appear and sometimes dementia. In the last stage of the disease, the patient may not even stand or walk, leading to serious complications and death. The most common cause of death is idiopathic parkinson's disease followed by malignancy, ischemic heart disease, pneumonia and cerebrovascular disease [Pennington *et al*., 2010].

Nowadays, PD is the most common neurodegenerative disease in the world just after Alzheimer's disease. In 2019, it is reported that PD affected around 5 million people worldwide. The incidence in the young population is rather low but still existing, and it increases with age till the 3% on the population over 80 [Hayes, 2019]. The incidence of PD also varies with ethnicity, being highest in Hispanics, non-Hispanics Whites, Asians, and Blacks. Moreover, the rate for men is higher than for women [Stephen *et al*., 2003]. In addition, the symptoms are different, less degenerative and later on time [Miller & Cronin-Golomb, 2010]. Gender differences are reflected in a 3:2 ratio. In women, the tremor is usually the dominant symptom. The initial symptom in men is usually the bradykinesia and the tremor-dominant form is associated with a slower disease progression. The only functional and statistically reliable protective effect against PD is the action of estrogen on the nigrostriatal dopaminergic system [Martínez-Rumayor *et al*., 2009].

The *substantia nigra* (SN) is one of the most important parts of the brain as the cells of this region are in charge of the dopamine (DA) production, and so it is involved in PD development. The SN is a long nucleus located in the midbrain and it is connected to the nuclei of the basal ganglia. It is divided in two regions: the *pars compacta*, which contains the cell bodies of dopaminergic neurons, and the *pars reticulata*, which consists on GABAergic neurons. The degeneration of the *pars compacta*

found in PD patients is associated with a decrease on the DA physiological concentration [Zhang *et al*., 2017]. The reduction of dopaminergic innervation to the striatum results in reduced movements and hypokinesia.

1.1.1. Etiology

Parkinson's disease is an extremely heterogeneous disorder, and its etiology is not completely understood. There are different factors, both environmental and genetic, that may increase the risk of developing it. Environmental factors include exposure to contaminated water, pesticides, herbicides, industrial chemicals, and wood pulp mills. Moreover, different toxins have been associated with the development of PD. Trace metals, organic solvents and carbon monoxide in the case of exogenous toxins, and tetrahydroisoquinolines and β-carbolines in the case of endogenous toxins [Olanow & Tatton, 1999].

The hypothesis proposed by Olanowet & Tatton (1999) states that the pathological process starts with the formation of proteinaceous intraneuronal Lewy bodies (LB) and Lewy neurites (LN) in the dorsal motor nucleus of the vagus nerve and in the anterior olfactory structures. Then, they progressively invade the brain, starting with the SN until they reach the neocortex in the last stage. LBs are intracellular pathological amyloid inclusions, which in PD are composed mainly by α-synuclein (αSyn) aggregates that accumulate in the soma. The LNs are the axonal accumulation of αSyn amyloid fibrils that contribute, together with LBs, to the reduction of the repair function in neurons, which, in time, triggers cell death. The dorsal motor nucleus of the vagus nerve is in charge of the parasympathetic control of the heart, lungs and digestive tract. Together with the anterior olfactory structures, they control olfactory and digestive tracts, which highly interact with the environment. Toxicants such as air pollutants, pesticides or viruses can enter the individual through these pathways and initiate PD pathogenesis. The olfactory pathway represents an entry point for pollutants that bypasses the blood-brain barrier, and this could also be a potential route for the pathogenic form of αSyn. This hypothesis also states that microbiome is implicated in the PD development as it seems that gut enteric nerves are initiating sites for the pathology [Chen & Ritz, 2018]. With time, pollutants and pathogenic forms of αSyn reach the brain, leading to dopaminergic neuron death in the SN.

1.1.2. Current treatments

In the past years, different treatment options were studied to reduce symptoms associated with PD. These therapies were based on the use of marijuana, lithium or electroconvulsive shock therapy. All these possibilities are related to important side effects, like addiction or physical damages. Moreover, they didn't intervene in the disease process [Elsworth, 2020]. One of the best ways to treat PD is increasing DA concentration in the body with the administration of L-dihydroxyphenylalanine (L-

DOPA) [Yuan, 2010]. This molecule is a blood-brain-barrier-permeable DA precursor which is converted into DA in the *pars compacta* region of the *SN* by the DOPA-decarboxylase. However, if the administration of L-DOPA occurs orally, it is converted by the DOPA decarboxylase into DA at a peripheral level and this is associated with side effects like vomiting, nausea, arrhythmia and postural hypotension. Therefore, inhibition of enzymes involved in the DA catabolism have to be formulated together with DA.

To treat PD, the drugs are usually co-administered, but this approach is often compromised by low patient compliance. Moreover, the combination of different molecules could produce different degrees of pharmacokinetics and pharmacodynamics profiles and it might also cause combined toxicity and side effects due to drug–drug interactions. As a matter of fact, in the last years the need to create new drugs formed by a single ligand that can modulate different specific targets at the same time increased. However, the excessive promiscuity of multi-target drugs could be related to unwanted reactions due to the interaction of them with molecules which are not the targets. To fix the problem, they are designed to present specific activity against the desired target and this reduces the risk of off-target activity. The most effective of them is ladostigil, which is a dual cholinesterase–monoamine oxidase-B inhibitor, designed by combining the carbamate cholinesterase inhibitory moiety with the MAO inhibitory propargylamine moiety from two different drugs [Van der Schyf, 2011]. However, the actual treatments do not cure the PD but only delay its worst symptoms.

1.2. α-Synuclein

α-Synuclein is a small presynaptic peripheral membrane protein highly expressed in the central nervous system, where it constitutes about the 0.5-1.0% of the entire cytosolic protein content. In its fibrillar form, it constitutes intracellular deposits of proteins and lipids defined as Lewy bodies (LB) and Lewy neurites (LN), which can be considered as one of the hallmarks of PD and other related neurological disorders [Spillantini *et al*., 1997 & 1998]. αSyn is part of the Synuclein's family, which are proteins abundantly present in the brain, binding to phospholipid membranes [Clayton & George, 1998]. There are three types: α-synuclein, β-synuclein and γ-synuclein. They share around 55-62% of their amino acid sequence and are composed by 140, 134 and 127 amino acids, respectively. They also have a similar domain organization [Lavedan, 1998].

1.2.1. Structure

αSyn is composed by three domains: The N-terminal lipid-binding α-helix domain, the amyloid-binding central domain (NAC), and the C-terminal acidic tail [Ememzadeh, 2016]. The N-terminal domain takes the 87 first residues. It is a positively charged region, including seven repeated series of

11 amino acids. This repeat contains a highly conserved KTKEGV hexameric motif that is also present in the α-helical domain of apolipoproteins. Moreover, the ability of αSyn to disrupt lipid bilayers is related to these repeated sequences by inducing the formation of α-helix, and subsequently reducing the tendency to form β-structures. The core region of αSyn (residues 61-95), also known as NAC, is involved in fibril formation and aggregation as it can form β-structures [Rodriguez *et al*., 2015].

The C-terminal domain of αSyn (residues 96-140) is an acidic tail of 43 amino acids, containing 10 Glu and 5 Asp residues. Structurally, this domain is present as a random coil due to its low hydrophobicity and high net negative charge. *In vitro* studies have revealed that αSyn aggregation can be induced by the reduction of the pH, which neutralizes these negative charges [Ahn *et al*., 2006; Hoyer *et al*., 2002]. An interaction between the C-terminal domain and the NAC region is thought to be responsible for the inhibition of αSyn aggregation. Moreover, in the presence of Al^{3+}, the C-terminal domain binds to this metal ion, ruining the inhibitory effect, and leading to aggregation. The phosphorylation of the ^{129}Ser is important in this inhibitory effect, and so its dephosphorylation leads to aggregation [Esposito *et al*., 2007]. In addition, the C-terminal domain of αSyn is homologous with small heat shock proteins, suggesting a protective role for αSyn in keeping proteins out of the degradation process [Kim *et al*., 2004].

Pathological structure

Opposed to its physiological conformations, under pathological conditions αSyn adopts a β-sheet amyloid structure: this change is associated with aggregation, fibril formation, and LB deposition [Conway *et al.*, 1998, & 2000; El-Agnaf *et al.*, 1998; Narhi *et al.*, 1999; Rochet *et al.*, 2000; Ding *et al.*, 2002; Lashuel *et al.*, 2002; Greenbaum *et al.*, 2005; Fredenburg *et al.*, 2007; Uversky, 2007; Yonetani *et al.*, 2009]. αSyn can be subjected to multiple post-translational modifications, including phosphorylation, oxidation, acetylation, ubiquitination, glycation, glycosylation, nitration, and proteolysis. All of these PTMs lead to changes in αSyn's charge and structure, which in turn alters αSyn's hydrophobicity and binding affinities for other proteins, lipids and membranes.

1.2.2. Function

The physiological functions of αSyn are not well understood yet. However, it seems to interact with a variety of proteins and cellular components [Burré *et al*., 2018]. The first function of αSyn concerns lipid transport, lipid packing and membrane biogenesis: αSyn seems to be involved in the binding of fatty acids and in their transport between the cytosol and the membrane compartment [Lucke *et al*., 2006]. Being a lipid-binding protein, αSyn has been also shown to induce membrane curvature and to convert big, slightly-curved vesicles into highly curved vesicles [Varkey *et al*., 2010].

Moreover, αSyn was found to be an inhibitor of phospholipases D1 and D2, suggesting an involvement in membrane biogenesis and remodeling [Gorbatyuk *et al*., 2010]. Three observations lead to the hypothesis that αSyn might act as a molecular chaperone and bind other intracellular proteins. First, the structural and functional homology of αSyn with a family of molecular chaperone proteins [Ostrerova *et al*., 1999]. Second, the ability of αSyn to suppress the aggregation of thermally-denatured proteins through its C-terminus [Souza *et al*., 2000]; moreover, αSyn overexpression seems to protect dopaminergic neurons from oxidative stress and apoptosis [da Costa *et al*., 2000]. And third, in mice knocked-out for the CSPα co-chaperone, αSyn salvages the lethal neurodegeneration by assisting the assembly of the synaptic SNARE complexes [Chandra *et al.*, 2005; Burré *et al.*, 2010]. αSyn also seems to be involved in vesicles trafficking: in yeast, αSyn inhibits endoplasmic reticulum-Golgi trafficking [Cooper *et al*., 2006] and it induces aggregation of rab proteins leading to defects in endosomal trafficking [Soper *et al*., 2011]. In human, as it occurs in yeast, αSyn perturbs ER-Golgi trafficking [Gosavi *et al*., 2002], with a PD-involved mutation exacerbating the effect [Thayanidhi *et al*., 2010]. Another function of αSyn is dopamine synthesis and transport: by the reduction of the phosphorylation state of tyrosine hydroxylase (TH) and the stabilization of the dephosphorylated inactive TH [Wu *et al*., 2011], αSyn seems to inhibit dopamine synthesis by inhibiting TH's expression and activity [Yu *et al*., 2004]. In fact, it was observed that the age-related increase of αSyn in the *SN* was inversely related to TH expression [Chu *et al*., 2007]. Moreover, studies proved that αSyn affects the vesicular monoamine transporter 2 (VMAT2), a membrane protein that transports monoamine neurotransmitters from the cytosol to synaptic vesicles: in fact, the knock-down of αSyn increases VMAT2 density; on the contrary, the overexpression of αSyn inhibits the activity of VMAT2, causing a stop in dopamine homeostasis and an increase in its cytosolic levels [Guo *et al*., 2008]. Finally, αSyn seems to have a role in neurotransmitter release and synaptic plasticity: αSyn's presynaptic localization, its interaction with synaptic vesicles and its chaperone activity suggest that this protein might be involved in neurotransmitter release and synaptic plasticity. On the other hand, αSyn absence in worms and flies suggests the opposite. However, knocking out the three members of the synuclein family (α, β and γ) in mice shows changes in the structure of the synapses [Greten-Harrison *et al*., 2010] and an impairment in survival [Burré *et al*., 2010]: this, once again, suggests the involvement of αSyn in the maintenance of neurons. As for αSyn involvement in neurotransmitter release and synaptic transmission, the results of studies are conflicting. As *per* photobleaching experiments, αSyn is highly mobile in the presynaptic terminal and, upon stimulation, it disperses from synaptic vesicles [Fortin *et al*., 2005]. Therefore, αSyn modulates the mobility of synaptic vesicles between the synaptic terminals and aids in vesicles recycling [Scott *et al*., 2012]. αSyn also organizes into multimers at the synapses level: this leads to a clustering of vesicles and a subsequent restriction of vesicles motility which in turn decreases both endo- and exocytosis processes [Wang *et al*., 2014]. *In vitro* studies showed that αSyn

inhibits vesicle docking without impeding the fusion with the postsynaptic membrane [Lai *et al*., 2014], and that overexpression of αSyn causes accumulation of docked vesicles at the synapses level [Larsen *et al*., 2006]. Hence, αSyn's effect on neurotransmitter release is mediated rather by the regulation of vesicle stocks within the presynaptic button than by a direct effect on the release machinery.

1.3. α-Synuclein binding to membranes

Protein-membrane interactions are involved in virtually every aspect of cellular function, with fundamental roles in key tasks such as signaling, membrane trafficking between organelles and transport through cellular membranes. These tasks typically require interactions that are highly specific and regulated [Das & Eliezer, 2019]. To achieve this, IDPs have evolved to feature remarkable specificity in binding to various types of biological membranes through both hydrophobic and electrostatic interactions [Middleton *et al*., 2010]. This specificity is made possible by different membrane chemical properties (charged content, headgroup chemistry) as well as physical properties (membrane curvature, packing density). Membrane specificity is partly encoded in the primary sequence of an IDP but can also be modified or regulated by post-translational modifications [Das & Eliezer, 2019].

As mentioned, αSyn is a peripheral membrane protein (PMP); and, in contrast to integral transmembrane proteins (ITP), PMP display reversible binding to biological membranes. Most of the membrane-binding domains of PMP retain their tertiary structure in the unbound state; on the contrary, this does not occur in the case of IDPs, where radical structural changes occur due to the low energy barriers separating the different conformations. This enables such proteins to interact with diverse binding partners and respond to a variety of environmental stimuli. Moreover, IDP-membrane interactions may have a kinetic advantage in fast processes requiring rapid control of such interactions, such as synaptic transmission or signaling [Hurley, 2006].

Many IDPs gain structure when binding to protein partners, and this can also occur upon binding to biological membranes. Oftentimes, membrane-interacting intrinsically disordered protein regions (IDR) adopt a helical structure upon binding, undergoing a "folding-upon-binding" transition, where one surface of the helix is hydrophobic while the other is more hydrophilic. [Das & Eliezer, 2019]. Another line of control in the binding specificity is affected by factors such as the size of the helix residues and the positioning of those residues with respect to the interface, among other factors [Antonny, 2011]. However, some IDPs are also able to bind to membranes while remaining in their unstructured state, using individual side chains to interact with either the charged lipid heads or the hydrophobic environment inside the membrane bilayer. [Das & Eliezer, 2019].

Many models try to explain the folding and binding of IDPs to protein interactors. One of them is the conformational selection model, in which the correct and final conformation is chosen from a pool of different conformations once an IDP binds to its target. Another one is the induced fit model, in which binding to the membrane occurs first and it is followed by folding, which is therefore "induced" by the interaction. The so-called "fly-casting" model may be also considered an induced fit model. In fact, it is a stepwise process in which the initial binding of an IDP to an interactor promotes further folding events, which allows an IDP to have greater capture radius for binding when unfolded, even though with a lower affinity, followed by folding and consequent reduction in distance between the partners [Shoemaker *et al.*, 2000]. The common conformational selection that occurs in the case of structured proteins is rather rare for IDPs, since the secondary structure propensity determines the favored model, and IDPs usually lack a highly stable secondary structure in their free state. All told, it seems that the mechanism of "folding upon binding" is dependent on the specific system and does not appear to favor either model exclusively [Das & Eliezer, 2019].

Focusing on αSyn, studies of its binding to lipid vesicles have supported the induced fit model as binding mechanism. In particular, the N-terminal domain of αSyn binds to lipid membranes with a higher affinity than the rest of the protein. This is especially true for the physiologically relevant N-terminally acetylated form of the protein, for which the N-terminal 10 residues bind more tightly to lipid vesicles than the remainder of the protein [Dikiy & Eliezer, 2014]. Subsequent to lipid binding at the N-terminus, "folding upon binding" proceeds from the N- to the C-terminus of the lipid-binding domain. Studies on this matter showed that familial PD mutations that either interrupt helix formation (A30P) or disrupt lipid binding (G51D & V70P) [Bodner *et al*., 2010; Fares *et al*., 2014], presumably interrupt the propagation of the "folding-upon-binding" interaction. Interestingly, in the presence of such mutations, there is a reduction of the binding affinity of the C-terminal residues from the lipid binding domain to the mutation sites. And at the same time, there is an increase in binding affinity of the N-terminal residues to the mutation sites, suggesting some degree of anti-cooperativity in αSyn membrane binding [Ramezani *et al*., 2018].

Certain peripheral membrane proteins have the capability to specifically target highly curved membrane surfaces: one of these proteins is αSyn, by using its lipid binding domain [Middleton & Rhoades, 2010]. αSyn's curvature-sensing domain appears to be disordered in the absence of membranes [Davidson *et al*., 1998]. αSyn binds to membranes *via* its N-terminal lipid-binding domain, which is around 100 residues long and that includes the seven repeats containing the hexapeptide consensus KTKEGV. The domain acquires an amphipathic helix structure which is partially inserted into the lipid membrane; the Lys residues of the consensus sequence position themselves laterally towards

the lipid/water interface, allowing interaction with negatively charged lipid headgroups (*figure 1.5*) [Jao *et al*., 2008; Davidson *et al*., 1998, Segrest *et* al., 1974 & 1990; Eliezer *et* al., 2001]. The insertion of the hydrophobic face of a helix into the membrane interior is generally considered to favor positively curved membranes which feature an increase in packing defects capable of accommodating helix insertion. Moreover, the details of the side chain distribution on the different amphipathic helix faces appears to modulate curvature sensing [Antonny, 2011]. At the same time, electrostatic interactions can guide the IDP interaction with charged membrane surfaces; in particular αSyn, through its Lys-rich N-terminal region, mainly binds to membranes formed by negatively charged lipids.

An IDP can bind both to a curved membrane and to a flat membrane, always relying on the same properties and forces [Fusco *et al*., 2016]. Amphipathic helices that insert into one leaflet of a bilayer membrane can bend the membrane by a spontaneous local curvature mechanism [Zimmerberg & Kozlov, 2006]. Therefore, membrane remodeling can be associated with αSyn: this process is dependent on the lipid composition of liposomes/membranes and the ratio between protein/lipid of the mixture [Jo *et al*., 2000; Zhu & Fink, 2003; Madine *et al*., 2008; Bodner & Dobson, 2009; Varkey *et al*., 2010; Jiang *et al*., 2013].

1.3.1. Role of the N-terminal anchor in the α-Synuclein-membrane interaction

Different interaction mechanisms of αSyn with the membrane surface have been reported. It was suggested that the first 25 N-terminal residues of αSyn permit the membrane-anchoring process by allowing the initial association, while being important to the bound-unbound equilibrium. NMR data suggests that the N-terminal region resides on the surface of the vesicle without any insertion, [Fusco *et al*., 2014]; on the other hand, other articles suggest, using molecular dynamics simulations and NMR analyses, that the first 12-15 N-terminal residues are in part inserted in the bilayer, with a tilt angle of 12° [Pfefferkorn *et al*., 2012]. However, all of these considerations are dependent on the type of artificial membrane used, making the anchor region difficult to identify and characterize.

In a recently published work [Cholak *et al*., 2020], authors were able to isolate and characterize αSyn complexed with SUVs. In the cited article, it is reported that the N-terminal insertion of αSyn in anionic lipidic membranes and the subsequent α-helical structure formation enable membrane binding *via* avidity. In particular, *via* electrostatic attraction facilitated by the repetition of Lys residues embedded in the 11-mer motifs containing the hexapeptide consensus KTKEGV. Moreover, deletion of the first 14 N-terminal amino acids seems to inhibite αSyn-membrane interaction. In the same work, authors report that, introducing the 2-14 αSyn variant in mammalian cells, the protein seemed to avoid binding to membranes, highlighting once again the importance of the N-terminus.

According to Cholak and colleagues (2019), the N-terminus region directly interacts with membrane's head groups, increasing the probability of αSyn insertion in the bilayer because of a local concentration effect [Sorensen & Kjaergaard *et al*., 2019]. The hypothesis states that either the N-terminal tail inserts first into the bilayer, thus allowing cooperative folding of the remainder of the anchor region; or the α-helix is formed first, with the N-terminal tail following. Once one of these two possible events occur, the rest of the protein folds, leaving the C-terminal part unfolded and in its disordered state. Moreover, once the anchoring is established, N-terminal residues outside the anchor fold and unfold dynamically on the membrane surface. Thus, as shown on figure 1.2, it seems that αSyn binds to membranes trough a sort-of multilateral structure formed by the N-terminal tail (1-14) and a first helix, which both together form the actual anchor, and a second helix [Bodner *et al*., 2010].

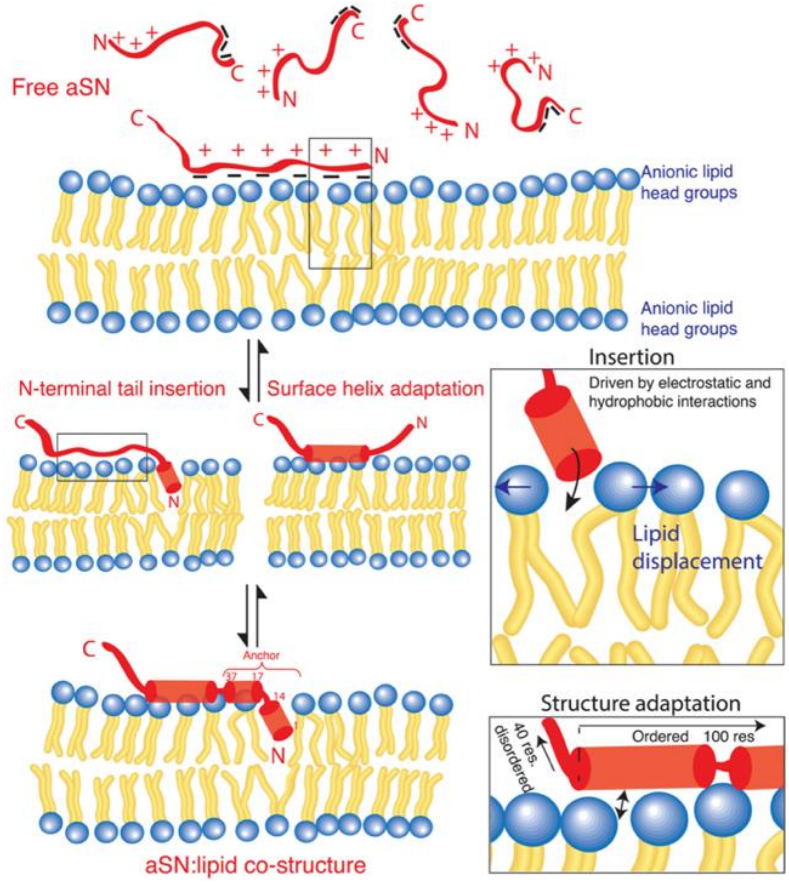

Fig. 1.1: *Cartoon of αSyn membrane interaction*. Initial electrostatic interactions lead the N-terminal and the Non-Amyloid-Component region of αSyn to approach the membrane's anionic lipid head groups. In the proximity of the lipid bilayer, the N-terminal tail inserts in-between the bilayer. The insertion enhances the local concentration, leading to folding-upon-binding of the remaining anchor helix. Avidity between the two events enhances the lifetime of the membrane-bound state and allows the remaining N-terminal to dynamically fold and unfold. The C-terminal remains disordered [Cholak et al., 2020].

In a cited study, upon SDS micelles formation, two helices were identified in αSyn [Ulmer *et al*., 2005]; this suggests the hypothetical use of SDS as membrane substitute, to perform initial experiments. Furthermore, the second helix was reportedly able to detach from a membrane and start novel interactions with a different one, leading to membrane fusion [Fusco *et al*., 2016].

1.3.2. Methionine oxidation effects on aggregation and membrane interaction

αSyn shows 4 Met residues in position 1, 5, 116, 127. Since αSyn's sequence does not include any Trp nor Cys residues, Met are the only residues which can be oxidized into methionine sulfoxides. αSyn's percentage of secondary structure elements seems to decrease upon synuclein's treatment with an oxidizing agent (αSynOx), thus maintaining the protein is its disordered conformation. This event might be due to the reduced hydrophobicity of the oxidized methionines [Glaser *et al*., 2005].

It is important to mention that αSynOx does not show propensity in amyloid fibril formation, which in turn leads to protein aggregation [Uversky *et al*., 2002]; moreover, it was reported that, upon addition of αSynOx in excess if compared to the native one, the Met-sulphoxide-containing protein seemed capable of preventing native αSyn fibrillation to a big extent. This suggests the presence of an interaction between the two αSyn species which leads to the formation of soluble oligomers rather than fibrils. The inhibition of fibrillation is proportional to the number of oxidized Met residues, and the effect seems to be equally distributed between the four residues. It is possible that, besides having an effect on fibril formation inhibition, Met oxidation may result in an alteration of αSyn's interaction with other cellular components [Glaser *et al*., 2005]. The accumulation of αSynOx leads to the formation of soluble oligomers that, if toxic, may increase the risk of developing PD. Therefore, cellular oxidative stress might hold a key role in the onset of the disease, besides its physiological role.

Native αSyn interaction with cellular membranes was discussed in section 1.3: oxidation of Met residues, on the other hand, reportedly leads to a decrease of membrane affinity of αSynOx [Maltsev *et al*., 2013]. The increase in hydrophilicity of MetOx1 and MetOx5, present in the membrane anchor, could be enough to avoid the hydrophobic interactions between the anchor and the membrane. Considering αSyn's involvement in membrane biogenesis, a more in-depth study of αSynOx-membrane interactions is needed.

2. Objectives

The aim of this project is to understand the role of the Met residues, specially the N-terminal one, in the biophysical properties of αSyn, with special attention to the interaction with lipidic membranes, which is an essential factor in PD development. For that, the objectives are:

- To set-up a production method for αSyn lacking the N-terminal Met residue (N-1-αSyn) by enzymatic approach.
- To provide a thorough biochemical and biophysical characterization of N-1-αSyn in comparison to αSyn and αSynOx, focusing on understanding their interaction with lipidic membranes.

3. Materials and Methods

3.1. Production of α-Synuclein, N-1-α-Synuclein and oxidized α-Synuclein

3.1.1. Recombinant protein expression

The production of αSyn was performed by means of recombinant protein expression. This technique allows the production and purification of large amounts of the protein of interest.

The expression was carried out in *E. coli* BL21 by using the expression vector pT7-7, a plasmid containing all the genetic information regarding the transcription and the translation of the protein [Tabor & Richardson, 1985]. Moreover, the expression vector includes the penicillin β-lactamase gene, which confers ampicillin resistance, enabling the selection of transformed bacteria by ampicillin exposure. In addition, αSyn is located just after the lactose (*lac*) operon, which helps to control the protein expression. Isopropyl β-D-l-thioga-lactopyranoside (IPTG) is a reagent that mimics the structure and function of allolactose, which stimulates the production of the *lac* operon. In this way, IPTG was used to achieve a high expression of the protein [Griffiths & Gelbart, 1999]. An osmotic shock protocol was used for protein extraction from the periplasm. αSyn's expression and purification protocol takes one week and it was performed several times to reach a sufficient amount of protein for all the studies. However, the insertion of the vector was carried out just once. The resulting transformed cells were divided and stocked at -80ºC in a 50% glycerol solution. Plasmid pT7-7 was purchased from Addgene (Watertown, Massachusetts, USA). The schematic structure of the vector containing the restriction sites and genes are reported in figure 2.1.

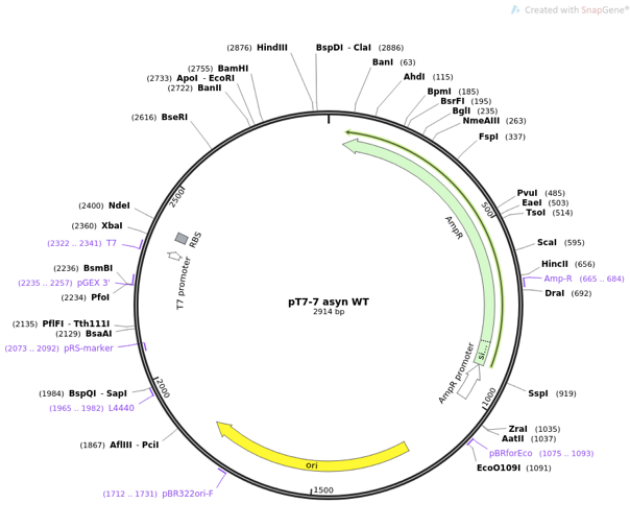

Fig. 2.1: *Plasmid pT7-7 used for the protein expression of αSyn in E.Coli [Paleologou, 2008].*

Transformation of BL21 competent *E. coli* cells was performed by a standard heat shock transformation protocol:

1. A bacteria aliquot of 200 µL was thawed in ice; 100 ng of plasmid were added to the solution. Bacteria were left on ice.
2. After 30 minutes, bacteria were incubated for 1 minute at 42ºC.
3. 400 µL of LB medium without ampicillin were added to the bacteria. They were incubated for 1 hour at 37ºC.
4. 150 µL of the solution were plated onto a Petri dish containing LB-agar with ampicillin concentrated 100 µg/µL. The plate was incubated overnight at 37ºC.

The expression and purification protocols are reported:

1. *Pre-inoculum*: transformed bacteria were added in a 250 mL flask containing 50 mL of LB with ampicillin concentrated 100 µg/µL. Bacterial cells were incubated at 37ºC under agitation.
2. *Inoculum and induction*: 28 mL of pre-inoculum were equally divided in two flasks of 2 L containing 750 mL of LB and ampicillin concentrated 100 µg/µL each. The flasks were incubated at 37ºC under agitation. Growth was monitored by OD evaluation: in particular, when the absorbance value reached 600 mAU, 375 µL of IPTG 1M were added to each flask.
3. *Pellet and osmotic shock*: after around 4 hours of induction, cell cultures were centrifuged at 4ºC for 10 minutes to obtain a bacterial pellet. Cells were then resuspended in 130 mL of osmotic shock buffer (40% sucrose, 30 mM Tris-HCl, 2 mM EDTA, pH 8.0). Samples were incubated at room temperature for 10 minutes. After a second centrifugation of 15 minutes, the pellet was resuspended in 130 mL of $MgCl_2$ solution.
4. *Boiling and refrigeration*: after the addition of 2.6 mL of Tris-HCl 20 mM, the supernatant was boiled for 15 minutes. The solution was centrifuged and the supernatant stored at 4ºC overnight.
5. *Salting out*: 19.4 g of $(NH_4)_2SO_4$ were added to every 100 mL of supernatant. The solution was stirred for 20 minutes on ice. After centrifugation, the same process was repeated with the addition of 11.8 g more of $(NH_4)_2SO_4$ for every 100 mL of solution: this led to a precipitate that was separated from the protein solution by an additional centrifugation step.
6. *Dialysis*: the pellet obtained by the final centrifugation was solubilized in 20 mL of Tris-HCl 20 mM buffer. The resulting solution was dialyzed versus deionized water for 2 hours at 4ºC by a dialysis membrane (cut-off 3.5 kDa). During the dialysis, the external phase was changed three times.

7. *Ion Exchange (IEX) Chromatography*: the resulting solution was filtered through a 0.22 µm PVDF membrane and then purified by IEX chromatography using a quaternary ammonium column (Resource Q, 6 mL). The elution gradient was performed with a 20 mM Tris-HCl, pH 8 solution (A) and a 20 mM Tris-HCl, 500 mM NaCl pH 8 solution (B). The gradient reached 100% of B phase in 30 minutes; αSyn eluted at 87% of B.
8. *Dialysis and Lyophilization*: the obtained solution was rich in salts, therefore it was dialyzed versus deionized water at 4ºC overnight. The solution was lyophilized, and the protein stored at -20ºC.

3.1.2. N-1-α-Synuclein production

N-1-α-Synuclein (N-1-αSyn) refers to the protein with the same amino acid sequence as the αSyn, but lacking the N-terminal methionine. Therefore, it is composed by 139 amino acid residues with a molecular weight of 14329.0 Da. N-1-αSyn was produced by enzymatic processing of the WT αSyn, using a recombinant methionine aminopeptidase from *Pyrococcus furiosus* (PfMAP), provided by Sigma-Aldrich (Saint Louis, MO, USA). PfMAP is a 32 kDa, thermostable metalloprotease belonging to the 2a class of methionine aminopeptidases, which specifically liberates the N-terminal methionine from proteins and peptides. *In vivo*, this kind of enzymes maintain protein homeostasis and coordinate post-translational modifications [Lowther *et al.*, 1999]. The structure of PfMAP elucidated by X-ray crystallography showed that the protein consists of a catalytic domain containing two cobalt ions in the active site and a unique insertion domain which is specific to the prokaryotic form of the protein [Tahirov *et al.,* 1998].

No data regarding the processing of αSyn by PfMAP was found in the literature. Moreover, the *in vitro* processing of the N-terminal Met by PfMAP and EcMAP (*E.coli* MAP with very similar cleavage specificity to PfMAP), when the second residue corresponds to an Asp, as in the case of αSyn, was reportedly not occurring [Frottin *et al.*, 2006].

An *in vivo* study analyzing the N-terminal Met excision in all *E.coli's* proteins found that EcMAP catalytic efficiency increases when the maximum side-chain length of the penultimate amino acid decreases. In this direction, the percentage of proteins processed depending on the amino acid residue in the second position was calculated; the proportions ranged from 97.1% in the case of Gly to 0.0% in the case of the amino acids having a maximum side-chain length higher than 4 Å. It is important to note that there is a big reduction when overpassing the 3 Å, from the 71.0% of Cys (2.83 Å) to the 16.4% of Asn (3.68 Å). It is reasonable to imagine that the active center of EcMAP comprises one subsite specific for the N-terminal non-acetylated methionine and a second site, able to accommodate

the penultimate amino acid, provided that its maximal side-chain length does not exceed 4 Å. The occupation of this second subsite would be essential to trigger the peptide bond hydrolysis by the enzyme. In the case of Asp, with a maximum side-chain length of 3.74 Å, only the 16.1% of proteins present the N-terminal Met processed, following the maximal length rule [Hirel *et al.*, 1989].

Another *in vivo* study produced 20 different clones of *E.coli* expressing the human growth hormone in a way that the only variation between them was the second position of the N-terminus of the recombinant protein: Met-X-Glu-Glu. In the case of Asp, no processing of the Met was observed [Dalbøge *et al.*, 1990].

As the provider explains, one unit (U) of PfMAP hydrolyzes 1 µmol of methionine from a peptide with a primary structure composed by Met-Pro-Ala-Ala-Gly, in one minute at pH 7.5 at 37ºC. The specific activity provided is 0.5 units/mg of protein. The commercial solution containing the enzyme has the following composition: 0.01% Tween® 20, 0.1 mM $CoCl_2$, and 10 mM Tris-HCl, pH 7.5. A total of 200 µL, corresponding to 0.02 units of enzyme were acquired. Taking all the data mentioned, the amount of PfMAP available may be calculated with the following formula:

$$\boldsymbol{m = \frac{V \cdot C}{A}} \qquad \textbf{(2.1)}$$

Where *m* is the mass of the enzyme, *V* is the volume of the commercial solution provided (200 mL), *C* is the concentration of that solution (0.02 U/mL), and *A* is the specific activity of the enzyme (0.5 U/mg). The amount of enzyme obtained is 8 µg. Considering the volume, the concentration of the commercial enzyme is 0.04 µg/µL. This concentration was used for calculating the volume of the commercial solution that had to be used for each reaction.

The optimal enzymatic reaction conditions had to be set up by a series of experiments changing several factors, firstly to prove that the process was possible, and then to reach its highest yield. In total, three different mass-to-mass (m/m) ratios between PfMAP and αSyn were employed. These m/m ratios were then related with their equivalent enzymatic activity units (U) as a function of the amount of αSyn used (Table 2.1). The concentrations of the αSyn used were 1 µg/µL and 2 µg/µL.

Table 2.1. *Equivalence between αSyn:PfMAP m/m ratio and the µU / µg of αSyn.*

αSyn:PfMAP m/m ratio	µU / µg of αSyn
1:1000	0.5
1:10000	0.05
1:50000	0.01

In total, three buffers were tested in order to adjust the enzymatic activity (Table 2.2). The so-called *HEPES buffer* was selected as it was also used in a study monitoring the activity of the EcMAP with a coupled reaction with L-amino-acid oxidase and peroxidase [Frottin *et al.*, 2006]. As previously reported, PfMAP requires two Co^{+2} ions as cofactors to be biologically active: indeed, the selected buffer contains $CoCl_2$. HEPES is a zwitterionic sulfonic acid buffering agent with a negligible metal ion binding, which makes it a good choice for enzyme reactions that may be inhibited by metal chelation, as in this case. Potassium Phosphate Buffer (PPB) was also used, as it was proven to reduce the enzymatic activity of EcMAP [Boosman & Chang, 1987]. *RapiGest*™ SF buffer was employed to try to increase the stability of αSyn during the incubation. *RapiGest*™ SF is a surfactant used to enhance in-gel and in-solution enzymatic digestions of proteins. It is a mild denaturant that solubilizes and unfolds the substrate proteins, making them more susceptible to enzymatic cleavage without significantly inhibiting enzyme activity. Additionally, it is heat stable, therefore, it can be used in higher temperature digestions. Unlike other commonly used denaturants (e.g., SDS or Urea), *RapiGest*™ SF does not modify peptides or suppress endoprotease activity. This reagent is easily removed after use allowing MALDI-TOF MS, LC or LC/MS analyses of digested samples [Yu *et al.*, 2003].

Table 2.2. *Composition of the buffers used in the set-up of the method for N-1-αSyn production.*

Common name	Composition
HEPES	50 mM HEPES 0.2 mM $CoCl_2$ 150 mM NaCl pH 7.5
PPB	0.1 M K_3PO_4 $CoCl_2$ 0.2 mM pH 7.5
RapiGest™	*RapiGest* SF 0.1% NH_4HCO_3 50 mM $CoCl_2$ 0.2 mM pH 7.5

The temperature was set up at 37ºC, as the PfMAP commercial datasheet recommends. However, a temperature of 30ºC was also used as described in the study regarding the EcMAP [Boosman & Chang, 1987]; different incubation times were tested, ranging from 1 min to overnight. Two different inhibition processes were employed: a 2 minutes boiling water bath as described by Ben-Bassat A *et al.* (1987), which is expected to denature the enzyme; EDTA 3 mM was also used to block the reaction, which chelates the Co^{+2} ions that are essential for PfMAP's enzymatic activity [Boosman & Chang, 1987]. The presence of N-1-αSyn was analyzed by RP-HPLC and MS, separating the components of the samples and checking the mass of each of them, looking for the protein of interest.

When the N-1-αSyn production method was set up, a higher amount of αSyn was used to produce enough N-1-αSyn to perform all the other analyses: in particular, 500 µg of αSyn per reaction were processed.

3.1.3. Protein oxidation

Oxidized αSyn (αSynOx) was produced starting from lyophilized αSyn, following an oxidation protocol with hydrogen peroxide. αSyn aliquots were dissolved in 20 mM Sodium Phosphate (NaP) Buffer pH 7.4 and filtered through a 22 µm PVDF membrane. H_2O_2 solution was added at a final concentration of 4% and it was left for 20 min at room temperature, to allow the oxidation of αSyn's methionine residues. After 20 min, the protein solution was transferred to cellulose Amicon® Ultra 0,5 mL centrifugal filters (Merk Millipore Ltd., Ireland) and centrifuged at 15000 rpm for 10 min using a SCILOGEX SCI24 Micro-Centrifuge (Rocky Hill, CT, USA); after the first centrifugation, the eluate found at the bottom of the vial was discarded, NaP buffer was added to the 500 µL line and the column was centrifuged again at 15000 rpm for 10 min. At the end of this round of centrifugation, the eluate was discarded, NaP was added to the column, and the centrifugation procedure was repeated two more times. These steps of washing of the column are required to completely remove H_2O_2 from the protein solution: indeed, hydrogen peroxide is not retained by the column and flows through the filter, whereas the oxidized protein remains in the column. After the centrifugation rounds, the remainder of the solution (around 150 µL) was recovered with a pipette; the column was washed with 200 µL of NaP, which were then recovered as well. This step is necessary to ensure that all oxidized protein is recovered. αSynOx solution was filtered once again through a 0,22 µm PVDF membrane and protein concentration was determined by UV-Vis spectroscopy.

3.2. Polyacrylamide Gel Electrophoresis

Polyacrylamide gel electrophoresis (PAGE) was used to characterize the αSyn produced. This technique allows the separation of charged particles by means of a continuous current applied to an aqueous solution [Isbir *et al.,* 2013]. The presence of an electric field allows the migration of charged molecules towards the electrode bearing the opposite charge. The potential difference is the driving force, the application of a voltage leads to a resulting current flow that has an intrinsic resistance, which depends on the ionic strength of the medium. These parameters are linked thanks to the Ohm's law. Size, shape and charge of the species determine the electrophoretic mobility, which is the speed at which the molecules move through the medium between the two electrodes. The two most important parameters influencing this movement of molecules are the electric field (E) and the distance between the electrodes (d) (equation 2.2).

$$E = \frac{V}{d} \qquad v = \frac{E \cdot z}{f} \qquad \textbf{(2.2 \& 2.3)}$$

Thanks to equation 2.3, it is possible to calculate the electrophoretic mobility of specific molecules. Where *z* is the net charge of the molecules and *f* is the frictional coefficient. All the electrophoretic runs were carried out by a Mini-PROTEAN 3 electrophoresis cell (BIO-RAD Laboratories, Inc., Hercules, California, USA) employing hand cast acrylamide gel slabs. All the gel slabs were stained with a Coomassie solution and then distained, under continuous agitation, with a solution composed by 100 mL of ethanol, 150 mL of acetic acid and 1.75 L of deionized water.

3.2.1. SDS-PAGE

In the SDS-PAGE, the species loaded in the polyacrylamide gel are denatured and negatively charged. The combined use of sodium dodecyl sulfate (SDS) and a boiling step eliminates the influence of structure and charge, so that the proteins are specifically separated on the basis of their molecular weight. SDS acts as a surfactant, masking the proteins' intrinsic charge and conferring them very similar charge-to-mass ratios. Upon application of a constant electric field, the protein mixture migrates towards the anode, each protein with a different speed, depending on their molecular weight [Nowakowski *et al.*, 2014]. For sample preparation, the sample buffer, and thus SDS, is added in excess to the protein, and the sample is then heated to 95 °C for five minutes. The heating step disrupts the secondary and tertiary structures of the protein by disrupting hydrogen bonds and stretching the molecules. After cooling to room temperature, each sample is loaded into the well in the gel.

For this project a 13%T, 2.6%C, pH 8.8, acrylamide separating gel and a 5%T, 2.6%C, pH 6.8 acrylamide stacking gel were used. The running buffer was composed by 25 mM Tris, 250 mM Glycine and 0,1% SDS, pH 8,3. The electrophoretic run was performed at room temperature with a starting current intensity of 9 mA/slab, and then 12 mA/slab.

3.2.2. NATIVE-PAGE

The NATIVE-PAGE analyses proteins in their natural conformation. That means that the species loaded in the gel are separated according to their size, charge and conformational state. In this case, a 12%T, 2.6%C, pH 8.8, acrylamide separating gel, and a 5%T, 2.6%C, pH 6.8 acrylamide stacking gel without SDS were used to perform the electrophoretic run.

3.3. Chromatographic techniques

3.3.1. Reverse Phase – High Performance Liquid Chromatography

High performance liquid chromatography (HPLC) is based on the high-pressure pumping of the analyte (mobile phase) through a column containing an immobilized chromatographic packing material: the stationary phase. The properties of the sample and the solvent, as well as the nature of the stationary phase, determine the retention time of the analytes [Mikkelsen & Corton, 2004].

RP-HPLC is characterized by a high resolving power, which allows an optimal separation of the analytes based on their hydrophobic interactions with the stationary phase of the column. C4, C8 and C18 are the most common columns. They are composed of alkyl groups of 4, 8 or 18 carbon atoms, respectively; these are bound to a silica matrix *via* an ether linker with the silanol groups. The characterization of WT-αSyn and N-1-αSyn, as well as the purification of N-1-αSyn from its production process took place in a C4 column. Analytes establishing stronger interactions with the stationary phase exit the column later, when the gradient of the mobile phase is hydrophobic enough for them to change their hydrophobic interactions with the stationary phase for the hydrophobic interactions with the mobile phase. On the contrary, analytes showing lower hydrophobicity, and therefore lower interaction with the column, will elute earlier and will be characterized by shorter retention times.

The separation of the sample mixture is accomplished *via* an elution gradient, where the composition of the mobile phase changes over the course of the separation toward conditions favoring analyte dissociation from the stationary phase (Table 2.3). The combination of eluent A (trifluoroacetic acid 0.1% v/v in water) and eluent B (trifluoroacetic acid 0.085% v/v in acetonitrile) allows to change of the hydrophobicity of the mobile phase during the analysis. An increasing hydrophobicity is usually exploited for protein separation, which gives the name to this specific technique: “reverse phase”. The presence of a small amount of an acid increases the resolution of the peaks due to the ion pairs formed by trifluoroacetate and positively charged basic protein residues enhancing the difference of hydrophobicity between the species present in the sample. After the separation, the sample passes through a detection module, such as a fluorimeter or a UV-absorbance detector, which generates a signal correlated to the quantity of analyte emerging at a time.

All the analyses were conducted with a C4 column (Phenomenex 5 µm, 150 mm) with the gradient reported in table 2.3. The wavelength used by the UV-absorbance detector was 226 nm. The instrument used is a 1200 series Agilent Technologies (Santa Clara, California, USA).

Table 2.3. *Gradient method used in chemical characterization of the proteins by RP-HPLC.*

Time (min)	% of eluent B
0	5
5	5
10	38
25	43
27	90
31	90
32	5
38	5

3.3.2. Size-Exclusion Chromatography

Size-exclusion chromatography (SEC) is a ubiquitous technique for downstream processing of a protein product in modern biotechnology as well as for analytical assays. SEC is a type of partition chromatography in which molecules in solution are separated on the basis of their hydrodynamic volume, rather than by interaction with a stationary phase as the case of other chromatographies. In this case, the polymeric stationary phase contains pores of different sizes; the mobile phase is generally the same solvent used to dissolve the protein/analyte. The molecules have different degrees of access into the pores of the column: the ones with smaller size have higher penetration and larger molecules have less access to the matrix pores. The factors involved in the efficiency of the separation are the diameter and the pore size of the packing materials, the length of the column and the mobile phase flow rate. Selecting the proper eluent and stationary phase, as well as the pore size, is mandatory for a successful resolution. Analytes with a hydrodynamic volume (which can be related to the MW) smaller than a given pore in the resin can diffuse into it, while larger analytes are excluded. When a sample is applied to the SEC column, smaller analytes have access to a larger part of the total pore volume than larger solutes. As a result, smaller molecules will have a longer pathway during its elution through the pores, compared to the larger ones, which will elute directly without going through the pores [Mori & Howard, 1999].

This technique employs an isocratic elution with an aqueous buffer that allows the protein to remain in its native conditions. For this reason, proteins with the same MW but different structure will not show the same elution volume: therefore, a calibration of the column is needed before starting the elution of the analyte solution. It is performed with molecular standards of known MW, so that the MW of the analytes may be stimated [Saad & Seeman, 2002]. The three parameters V_r, V_o and V_i are used to describe the behavior of a molecule on a gel filtration column and these must be determined experimentally. The elution volume (V_r) is the volume that eluent and analyte need to pass through the column. The void volume (V_o) is the volume of interstitial liquid. Molecules with diameter

larger than pore size are completely excluded from the column and their elution volume is equal to void volume of the column. The inner volume (V_i) of the column is the total volume that the eluent can occupy in the whole column. It is equivalent to the sum of V_o and the volume of the pores. The behavior of a solute is described by its distribution coefficient (K_d) which is the fraction of V_i accessible to a solute molecule. The value of K_d will be zero for solutes totally excluded from the column. A K_d higher than 1.0 indicates adsorption or ionic interactions between solute and the gel material. It is possible to calculate the K_d of the species, in which the K_d is defined by the equation 2.4.

$$Kd = \frac{Vr - Vo}{Vi - Vo} \quad \textbf{(2.4)}$$

Therefore, molecular standards with known MW were loaded in the SEC column (Figure 2.2). Superdex 200 Increase 10/300 GL column was used in this project (Amersham Biosciences, Uppsala, Sweden). Blue dextran is completely excluded from Superdex and corresponds to the V_o.

Molecule	MW (kDa)
Dextran Blue	2000
TG	660
ApoF	479
AD	150
BSA	66.4
CA	29
RNAase	13.7
BPI	6.5

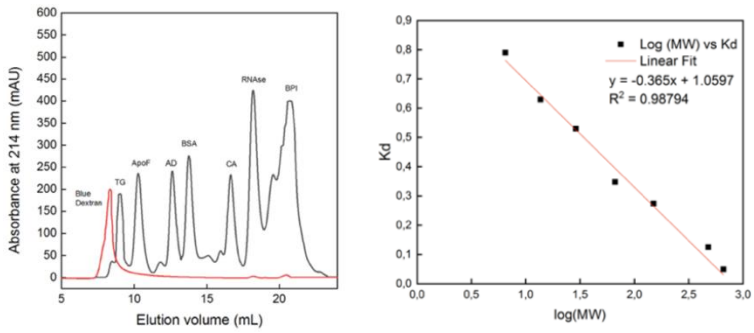

Table 2.4. (left) & Fig. 2.2 (right): On the left, the molecular standards used to calculate the calibration curve for the SEC analyses. In the middle, the SEC analysis for the determination of the calibration curve. The black line is relative to the SEC analysis of proteins and the red line is relative to the SEC analysis of Blue Dextran (Vo). Names of the species shown in figure are abbreviations of the proteins used: thyroglobulin (TG), apoferritin (ApoF), alcohol dehydrogenase (AD), bovine serum albumin (BSA), carbonic anhydrase (CA), ribonuclease (RNAase) and aprotinin (BPI). On the right, the calibration curve together with the linear equation extracted from it.

A calibration curve was made plotting the elution volume against the MW logarithm, from which an equation relating the linear correlation between V_r and log(MW) was obtained. It was also possible to plot the logarithm of the MW versus the K_d of the species, in which the diffusion constant is defined by the equation included in figure 2.2.

In this project, SEC was exploited for the characterization of WT αSyn and N-1-αSyn . All the analyses were carried out in an AKTA Fast performance liquid chromatography (FPLC) System (Amersham Biosciences, Uppsala, Sweden) connected to the Superdex 200 Increase 10/300 GL column. A 20 mM Tris-HCl, 150 mM NaCl pH 7.4 buffer was employed for the isocratic elution at a rate of 750 µL/min. The spectrophotometer detector was set at 214 nm for the peptide bond absorption.

3.3.3. Ion-Exchange Chromatography

Ion exchange chromatography (IEX) uses the FPLC system separating molecules on the basis of their respective charged groups. IEX retains molecules in the column based on their coulombic (ionic) interactions with the stationary phase. The matrix consists of positively or negatively charged ions, depending on the type of IEX employed: cationic or anionic exchange. To achieve electroneutrality, the charged groups of the stationary phase couple with the exchangeable counterions present in the mobile phase. Ionizable molecules that are to be purified compete with these exchangeable counterions for binding to the immobilized charges on the stationary phase [Amersham Biosciences, 2004].

For the purification of WT-αSyn following the production protocol, an anionic exchange column was used. The 6 mL RESOURCE Q column (GE Healthcare, Chicago, IL, United States), derivatized by quaternary ammonium, allows the interaction with the negatively charged C-terminal domain of the αSyn. The system is based on the use of two different eluents set up in a gradient: eluent A (20 mM Tris-HCl, pH 8) which allows the binding of the protein to the stationary phase due to its low ionic strength, and eluent B (20 mM Tris-HCl, 500 mM NaCl, pH 8) that gradually detaches the molecules from the resin increasing the ionic strength of the solvent that passes through the column. In this case, higher elution volumes mean higher interaction with the positively charged column and therefore higher amount of negative charges in the polypeptidic structure. On the contrary, lower elution volumes are due to lower amounts, or even non existing, negatively charged groups.

3.4. Mass Spectrometry

Mass spectrometry (MS) is a powerful analytical technique used to quantify known materials, to identify the components of a sample, and to elucidate the structure and chemical properties of different molecules [de Hoffmann & Stroobant, 2007]. The process involves the production of gaseous ions from the sample under investigation, which are then separated and characterized by their mass to charge ratios (m/z) and relative abundances. The instrument consists of three major components: ion source (produces gaseous ions from the substance under study), analyzer (separates the ions and/or their fragments and resolve them according to their m/z ratio) and detector system (detects the ions and records the relative abundance of each of the resolved ionic species).

There are different types of MS systems depending on the way they generate ions, separate and detect them. In this study, the MS analyzer used produces the gaseous ions by Electrospray Ionization (ESI). The analyte is injected into a small capillary that ends with a needle tip, which is maintained at high voltage (2.5 – 4 kV). The solution exits the needle as highly charged droplets

(aerosol spray) containing both solvent and ions. Then, a curtain of N_2 gas de-solvates the droplets, increasing the charge density till a point in which the repulsion force is higher than the addition of the surface tension and the solvation energy (Rayleigh limit). At this point, a Coulombic explosion occurs, which leads to the emission of isolated ions that will enter the analyzer [Kebarle & Verkerk, 2009]. The MS instrument used is composed by two types of analyzers: quadrupole (Q) and time-of-flight (TOF). The Q consists of four parallel cylindrical rods. A direct current voltage and a radiofrequency voltage are applied in opposite phases, inducing a zig-zag movement on the ions [Glish & Vachet, 2003]. At this point, only the ions with a determined m/z ratio in resonance with the electrodynamic field can go through the analyzer and reach the second analyzer. In the case of proteomics, as this one, two quadrupoles in a row must be used before the TOF. In the TOF analyzer, the ions derived from the Q are accelerated with a certain potential into a long tube under vacuum [Stafford *et al*., 1984]. The geometry of the tube is variable: the most important feature is its length, because the resolving power depends on it. After being accelerated, ions travel through the TOF tube. A reflectron equilibrates the kinetic energy of the ions with the same charge. At this point, as the potential energy applied is the same for all of the ions and it will be all converted into kinetic energy, which is directly proportional to velocity and mass, the ions with lower m/z ratio will reach a higher velocity than the ones with higher m/z ratio, and therefore, the time to cross the tube will be lower. This time is measured by the analyzer and related with the m/z ratio of the ion, which is shown, together with its relative abundance, in a chromatogram, as a MS analyzer output.

In particular, a Xevo ESI-Q-TOF spectrometer (Waters Corporation, Milford, Massachusetts, US) with a resolving power of about 10000 was employed. The mobile phase was a 0,1% formic acid aqueous-acetonitrile 1:1 solution. All collected data was processed and analyzed with MassLynx mass spectrometry software (Waters Corporation, Milford, Massachusetts, US).

3.5. Liposome and micelle production

Liposomes are small artificial sphere-shaped vesicles consisting of one or more phospholipid bilayers, that may also contain cholesterol, separating aqueous compartments. Their properties differ considerably with lipid composition, surface charge, size, and the method of preparation. Furthermore, the choice of bilayer components determines the ‘rigidity’ or ‘fluidity’ and the charge. Since liposomes are composed of naturally-occurring phospholipids, besides the many other applications in therapy and diagnosis, they are also excellent cell membrane models [Akbarzadeh *et al*., 2013].

Phospholipids spontaneously form closed structures when hydrated in aqueous solutions due to their amphipathic character. These liposomal structures are formed by one or more phospholipid bilayers, referred to as *lamellae* [Chrai *et al*., 2001]. Their diameter may vary from very small (0.025µm) to large (2.5µm) sizes. On the basis of the number of *lamellae* and diameter, they may be classified in either multilamellar vesicles (MLVs), formed by many unilamellar vesicles one into the other, separated by water compartments [Shaheen *et al*., 2006], or unilamellar vesicles (ULVs). ULVs may be further classified into either large unilamellar vesicles or small unilamellar vesicles (SUVs) [Amarnath & Sharma, 1997].

Liposomes can be obtained by several methods, the most common ones being extrusion and sonication, each yielding liposomes with different sizes and size distributions [Lapinski *et al*., 2007]. Extrusion was the chosen technique for the generation of SUVs, which is the most suitable method for producing ULVs. With extrusion, a lipid suspension is forced through a well-defined pore size membrane to produce vesicles with a diameter near the pore size of the membrane. Extrusion avoids the need to remove organic solvents and detergents from the final lipid preparation and can be applied to a wide variety of lipid species and mixtures. Another huge advantage is the fact that is a reasonably reproducible technique resulting in a proper average size with a low distribution.

In particular, the Morrisey Lab Protocol for Preparing Phospholipid Vesicles by Extrusion was used. Phospholipids stock solutions (Avanti Polar Lipids) were dissolved in chloroform: L-alpha-phosphatidylcholine (egg, PC) and L-alpha-phosphatidylserine (bovine liver, PS). The starting liposomal suspension was prepared at a concentration of 8 mM (6.33 mg/mL) under the chemical hood with a formulation m/m PC:PS 1:1. The phospholipid (PL) mixture was then dried under a gentle N_2 gas stream, rotating the vial, to allow PL to be absorbed onto the vial's glass walls. Once dried, the obtained gelly-like residue was placed in a SpeedVac vacuum concentrator (Thermo Fisher Scientific, Waltham, MA, USA) for one hour and a half under high vacuum, to allow the PL pellet to be entirely dried. After that, 1 mL of 20 mM NaP buffer pH 7.4 at 37ºC was added, the vial sealed and incubated 1 hour at room temperature. Then, the tube was vortexed to completely resuspend the PL mixture, resulting in a milky, uniform suspension. The following step was a 5-cycles freeze-thaw treatment: the suspension was kept at 37ºC for 2 minutes, vortexed and frozen by using ice mixed with $CaCl_2$ to decrease even more the temperature of the ice. For what concerns the extrusion procedure, the Liposofast device (Avanti Polar Lipids) was used. It was assembled with two filter supports held between the two "O" rings and a 0.1 µm membrane in between the filters. Before starting with the extrusion procedure, the two syringes were washed with the NaP buffer in which the liposomes were resuspended. The two filters were wetted with MilliQ water. Avoiding air bubbles, the liposome suspension was transferred

from the glass tube to one of the two Hamilton syringes, which was then attached to the Luer lock on one side of the device. The other (empty) syringe was attached to the Luer lock on the opposite side of the device, which was then inserted into its stand to keep it from moving. The loaded syringe's plunger was pressed to pass its entire contents through the filter and into the opposing syringe. The process was repeated alternatively with the two syringes for a total of 11 passes; it is important to use an odd number of passages, so that the final product will end up in the originally empty syringe. This will ensure that none of the starting MLVs contaminates the final product. The final SUVs produced were transferred to an Eppendorf and characterized by dynamic light scattering.

3.6. Spectroscopic techniques

3.6.1. Dynamic Light Scattering

Dynamic Light Scattering (DLS), also known as photon correlation spectroscopy, is a very powerful tool for studying the diffusion behavior of macromolecules in solution, which is related to their size [Berne & Pecora, 1976]. When a monochromatic beam of light encounters a solution containing macromolecules, light scatters in all directions as a function of their size and shape, and the scattering intensity is recorded by a detector. The monochromatic incident light then undergoes a phenomenon called Doppler broadening as the macromolecules are in continuous motion in solution (Brownian motion) due to the bombardment by solvent molecules that surround them; the larger the particle, the slower the Brownian motion. Therefore, DLS measures fluctuations of intensity of diffused light and relates it with their Brownian motion and their size [Stetefeld *et al.,* 2016].

During a DLS measurement, the sample is illuminated by a laser beam: the intensity variations of the scattered light are collected as a function of time by a detector positioned at a fixed angle Θ (normally 90°) and connected to an analysis software. The scattered light undergoes either constructive or destructive interference by the surrounding particles: the fluctuations in intensity reflect the time scale of movement; as a result, light will be scattered at a certain intensity, which is detected [Pecora, 1985]. It is important to maintain a known and stable temperature, since knowledge of the solution viscosity is required; at equal temperature and viscosity conditions, small particles move rapidly inducing rapid variations in the scattering intensity; on the other hand, larger particles move slowly inducing slow intensity variations. By measuring the variations and their fluctuations, an autocorrelation function determines the D_T (translational diffusion coefficient), which defines the Brownian motion. The correlation function used to derive the D_T is the following:

$$\boldsymbol{G(\tau) = A \cdot (1 + B \cdot e^{-2DTq^2\tau})} \qquad \textbf{(2.5)}$$

Where G(τ) is the autocorrelation function, A is the function base line, B is the intercept of correlation function, q = [(4πn /λ_0)senΘ], n is the refraction index of the medium, λ_0 is the laser beam wavelength and Θ is the scattering angle. The equation correlates intensity of scattered light with the delay of the intensity signal due to the diffusion of particles. Once D_T is calculated, it is possible to calculate as well the hydrodynamic diameter of the particle under study with the Stockes-Einstein equation:

$$\boldsymbol{DT = \frac{kb \cdot T}{6\pi\eta Rh}} \quad \textbf{(2.6)}$$

Where DT is the diffusion coefficient, kb is the Boltzmann coefficient (JK^{-1}), T is the temperature, and η is the viscosity of medium [Stetefeld *et al*., 2016]. The heterogeneity of data occurs because of the fact that bigger molecules scatter a higher amount of light with respect to the smaller ones, as the intensity of diffused light is directly proportional to the particle's diameter. In order to obtain more precise data, it is generally preferred to evaluate the hydrodynamic results for the volume instead of for the intensity distribution.

For this project, a Zetasizer Nano-ZS instrument, Malvern Panalytical (Malvern, Worchestershire, United Kingdom) was used. To characterize liposomes and monitor their stability, 100 µL of liposomal suspensions were loaded in ZEN0040 disposable cuvettes and analyzed at 25ºC with an automatic setting, and a total of 3 measurements were performed to have average values. Liposomes were not diluted during the evaluations, but were analyzed at their specific concentration.

3.6.2. UV-Visible Spectroscopy

UV-Visible spectroscopy (UV-V) measures the absorbance of this type of light by a certain sample. Absorption of the UV-visible radiations results in the excitation of the electrons from lower to higher energy levels. In organic molecules, only certain functional groups (chromophores), which contain valence electrons of low excitation energy, can absorb ultraviolet and visible radiation. This technique allows quantitative and qualitative analyses. In this project, it was used for protein quantification before starting each analysis, as well as for checking the presence of αSyn in the last steps of its purification process. In particular, the absorbance spectrum of 350-230 nm was evaluated. Its shape is particular for α-Syn, so it also serves as a checkpoint before starting the analyses. Then, the absorbance considered for the quantification was the one at 280 nm subtracting the one at 350 nm, in order to avoid considering possible contaminations. All analyses were carried out with a Lambda-25 spectrophotometer from Perkin Elmer (Shelton, CT, United State), using a 1 cm pathlength quartz cuvette of 100 µL.

To calculate the concentration of αSyn and N-1-αSyn , their extinction coefficient (ε) was determined using the one of Tyr at 280 nm, which is the only amino acid residue present in αSyn that absorbs at that wavelength (equation 2.8).

$$\varepsilon M, protein = 2Tyr \cdot \varepsilon M, Tyr \quad (2.8)$$

Where η is the number of residues present in the protein. And εM is the specific molar extinction coefficient of the Tyr (εM,Tyr = 1.490 M^{-1} cm^{-1}). Considering that there are four Tyr in α-Syn, its molar extinction coefficient (εM) is 5.960 M^{-1} cm^{-1}, and considering its MW, its ε is 0.412 μL μg^{-1} cm^{-1}. In the case of N-1-αSyn , the εM is the same of the one of the WT. However, as it has one less amino acid residue, the MW is different, and so it is the ε (0.416 μL μg^{-1} cm^{-1}). The protein concentration was then evaluated thanks to the Lambert-Beer law (equation 2.9), where A is the absorption, L is the optic pathlength (1 cm), and c is the concentration of the sample solution [Stanley & Peter, 1989].

$$A = \varepsilon \cdot L \cdot c \quad (2.9)$$

3.6.3. Circular Dichroism

Circular dichroism (CD) is a spectroscopic technique that may be used to qualitatively measure the secondary structure of proteins; it may also serve for studying the tertiary and quaternary structures: conformational changes, folding degree and protein-protein interactions. CD refers to the differential absorption of the left and right circularly polarized components of plane-polarized radiation. This effect occurs when a chromophore is chiral (optically active) either intrinsically by reason of its structure, or by being covalently linked to a chiral center, or by being placed in an asymmetric environment [Kelly & Prince, 1997]. Therefore, CD is exhibited by biological molecules because of their dextrorotatory and levorotatory components. The CD spectrum may be measured as a function of wavelength in two possible ranges: near-UV (320-260 nm) and far-UV (240-180 nm).

Electromagnetic radiation consists of an electric and a magnetic field that oscillate perpendicularly one to the other. Linearly polarized light occurs when the electric field vector oscillates only in one plane; circularly polarized light, instead, occurs when the electric field vector rotates on its propagating direction while the magnetic field vector remains constant in magnitude [Rodger, 1997].

The far-UV spectra of proteins are dominated by n → π* and π → π* transitions of amide groups; intensities and energies associated to the transitions in peptide bonds depend on ϕ and ψ angles, hence on protein conformation. The peptide bond is the principal absorbing group; therefore, CD in far-UV provides information on the way the peptide bonds are organized, which reliably

stimulates the secondary structure content of the protein, in terms of proportions of α-helix, β-sheet and random coil; however, it does not indicate which structure corresponds to each region of the protein. Far-UV CD spectra is the result of the algebraic sum of signals due to the single secondary structures; therefore, it is the average curve. It informs about the nature of the structure which is mostly present [Kelly & Prince, 1997].

In the near-UV, aromatic amino acid side chains of phenylalanine, tyrosine and tryptophan absorb in the range between 250 to 290 nm [Kelly & Prince, 1997]. The folding of the protein places the side chains of the aromatic acids in a chiral environment, which gives rise to a CD fingerprint spectra characteristic of its native structure. In proteins containing disulphide bonds, the dihedral angle of this bond can also give a signal, thus contributing to the fingerprint spectra. Unlike far-UV CD, near-UV CD spectrum cannot be assigned to any particular 3D structure, it is peculiar to each polypeptide structure.

During a CD experiment, circularly polarized light passes through the sample which is placed in a cuvette; because of this, optically active molecules will not equally absorb the two polarized radiations (A_L and A_R). In more detail, the different absorption produces an elliptical polarization of the outcoming radiation, as shown in the following equation:

$$\Delta A = A_L - A_R \qquad \textbf{(2.10)}$$

Most measurements, however, are reported in degrees of ellipticity (θ) which is the *arc tangent* of the ratio between the minimum semi axis and the maximum semi axis of the polarization ellipse. Ellipticity is also correlated to the differential absorption by the following equation:

$$\vartheta = 32{,}98 \cdot \Delta A \qquad \textbf{(2.11)}$$

To estimate proteins' and polypeptides' secondary structure, the measured molar ellipticity spectrum has to be normalized to a value independent from the polymer's length. Therefore, mean residue ellipticity [θ] is used; it is calculated by dividing the measured molar ellipticity of the molecule by the number of monomer units (residues).

$$[\theta] = \frac{\theta obs \cdot MRW}{10 \cdot l \cdot c} \qquad \textbf{(2.12)}$$

In this equation, θ_{obs} is the ellipticity observed, *l* is the pathlength, *c* is the protein's concentration in the sample and MRW is the protein's mean residue weight.

Keeping these principles in mind, it is possible to determine the secondary structure of proteins using CD. When the chromophores of the amides of the polypeptide backbone are aligned, their optical transitions are shifted or split into multiple transitions. The result is that different secondary structure elements have characteristic CD spectra. The dichroic signal detected at wavelengths in the far-UV is due to the absorption of peptide bonds, made asymmetrical by the clarity of the adjacent α-carbon. Since the electronic transitions of these chromophores are sensitive to the conformation geometry, the absorption spectra of a random coil, α-helix or a β-sheet are different (Fig.2.3).

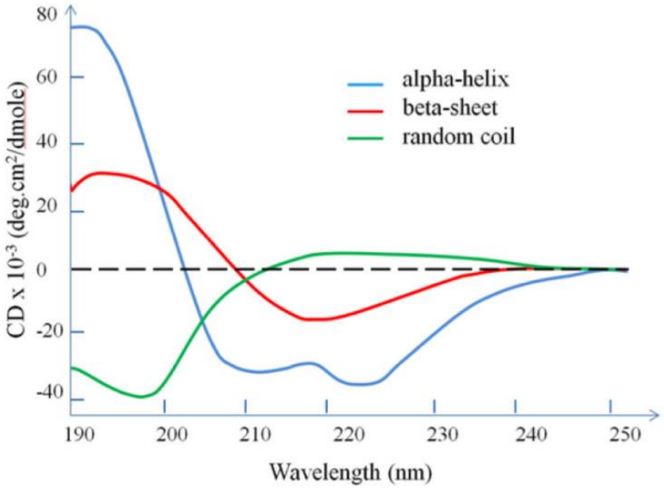

Fig. 2.3. *Standard CD profiles of α-helix (blue), β-sheet (red) and random coil (green) used to characterize the secondary structure of the proteins by comparison.* The spectrum of an α-helical structure is characterized by a negative band at 222 nm due to the *n* → π* transition, a negative band at 208 nm, and a positive band at 190 nm due to the π → π* transitions. The structure with β-antiparallel sheets is instead characterized by a negative band at about 220 nm due to the *n* → π* transition and by a positive band at 200 nm due to the π → π* transition. The n → π* transition of the random coil structure manifests itself as a weak positive band at 218 nm, while the π → π* transition manifests itself as an intense negative band at 197 nm. [Wei *et al.,* 2014].

In this project, CD was used to evaluate the structural changes occurring in αSyn, αSynOx and N-1-αSyn in the presence and absence of liposomes and SDS. A Jasco J-170 spectropolarimeter (Tokyo, Japan) was used to monitor the proteins' structural changes, working in the far-UV spectrum between 250 nm and 195 nm. Analyses were carried out using a 1 mm pathlength quartz cuvette; protein samples were analyzed at a concentration of 0.1 mg/mL in 20 mM Sodium Phosphate buffer, pH 7.4. Liposomes and SDS were also present in the samples, in the case of liposomes, in a m/m ratio 1:10 and, for what concerns SDS, 10 mM (above its critical micellar concentration - CMC). Spectra acquisitions were performed using the following parameters: 100 mdeg (standard), continuous scanning mode at 20 nm/min, response of 16 seconds, band width 2 nm and 2 accumulations.

4. Results & Discussion

4.1. Production of α-Synuclein, N-1-α-Synuclein and oxidized α-Synuclein

4.1.1. Expression and purification α-Synuclein

The expression of αSyn was carried out by *E. coli* transformed with pT7-7 plasmid (Fig. 2.2). Since the proteins are mostly located in the periplasmic space, the extraction was performed following the osmotic shock protocol. The expression and purification procedures were monitored by SDS-PAGE electrophoresis (one of them is represented in the figure 3.1). Aliquots of each step were collected and then mixed with sample buffer.

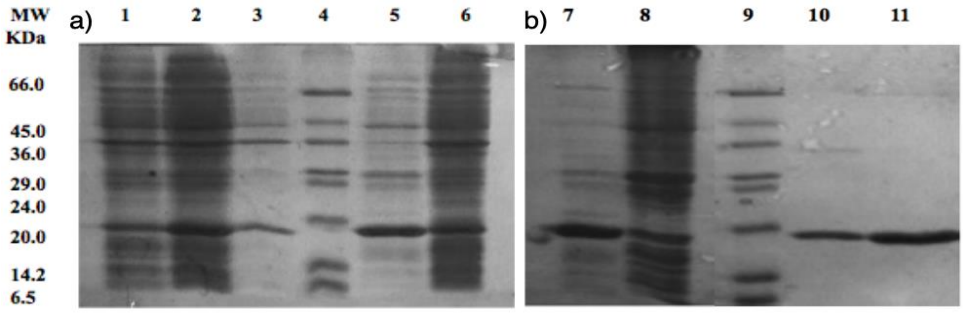

Fig. 3.1. *SDS-PAGE gel electrophoresis of the expression and purification steps of αSyn from E. Coli*. For the analysis 13% acrylamide gels were employed. In each well 7 µL were loaded. Lane 4 and 9: molecular weight markers. The other lanes are the solution from the purification in chronological order. Lane 1-2: E.coli culture before and after the induction. Lane 3: post-centrifugation pellet after resuspension. Lane 5-6: post-centrifugation supernatant and pellet after osmotic shock treatment. Lane 7-8: post-centrifugation supernatant and pellet after boiling. Lane 10: post-centrifugation supernatant after the ammonium sulphate precipitation. Lane 11: sample collected post-FPLC.

In figure 3.1, all the purification steps are displayed. It can be appreciated an increase of thickness of the αSyn band, around 20 kDa. All the other bands in the gel represent the species present in bacterial cells. During the boiling and the precipitation with ammonium sulphate steps (Fig. 3.1 lanes 6 and 8 respectively) the majority of the contaminants were removed. The protein was then characterized by RP-HPLC and the corresponding pick was then analyzed by MS to check its purity and identity (Fig. 3.2).

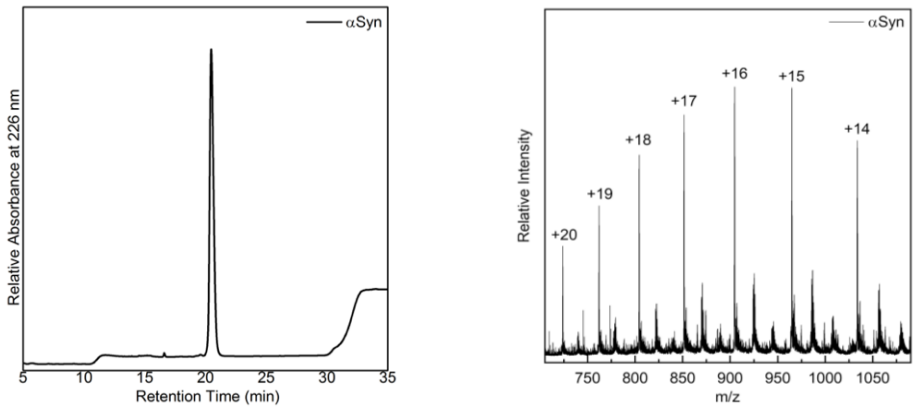

Fig. 3.2. *Idetification and characterization of αSyn*. The chromatogram on the left shows the RP-HPLC analysis with the αSyn eluting at 20.8 min. The one on the right shows the MS analysis .

4.1.2. Production of N-1-α-Synuclein by enzymatic processing: Set-up of the method

In the first analysis, HEPES buffer was employed at an m/m ratio of 1:1000, incubating at 37ºC for different times. The reaction was inhibited with a two minutes boiling water bath and the product kept in the fridge for two days before the MS analyses. The resulting chromatogram showed that the αSyn was entirely degraded. As it could have been due to the high ratio PfMAP:αSyn, which could lead to a loss of the enzymatic specificity, the same experiment was performed changing to lower ratios (Table 3.2. Exp. B & C). However, the result did not change. It could have been because of the buffer used, which could be increasing the activity of the enzyme till a point that it became non-specific. Another idea was that perhaps the inhibition process was not successful and the reaction kept going for the two days that the samples were in the fridge. Therefore, a fourth experiment (Exp. D) was set up using PPB, which was proved to reduce the enzymatic activity of EcMAP. The inhibition process was also changed to EDTA 3 mM to slow down the reaction by chelation of the Co^{+2} ions, which are essential for PfMAP's enzymatic activity and was also proved to work in the same study [Boosman & Chang, 1987]. From this point on, the analyses were followed by RP-HPLC. In this way, the time in which the results were obtained as well as the time in which the reaction product was kept in the fridge was considerably reduced and the analyses were always performed on the same day. The peaks corresponding to retention times between 20 and 35 minutes were recovered for MS analyses in order to check the nature of the molecules eluting at those times. The peak corresponding to the αSyn in HPLC was analyzed to check the hypothesis stating that N-1-αSyn co-eluted with αSyn, which was discarded. As there was not cut at all in exp. D (Fig.3.3), a higher m/m ratio was employed without further success (Fig.3.3. Exp.E).

At this point, the enzymatic activity required to be increased, so HEPES buffer was used again in exp. F at different m/m ratios but same incubation time (1h). In this case, the temperature was set at 30ºC as they also established in the study previously mentioned. The enzymatic activity was still not shown, therefore, in exp. G, the reaction was run overnight with the two buffers that had already been used. The one in HEPES buffer showed a different chromatogram, with a small peak just after the common αSyn peak, which was confirmed to be N-1-αSyn by MS (Fig. 3.3).

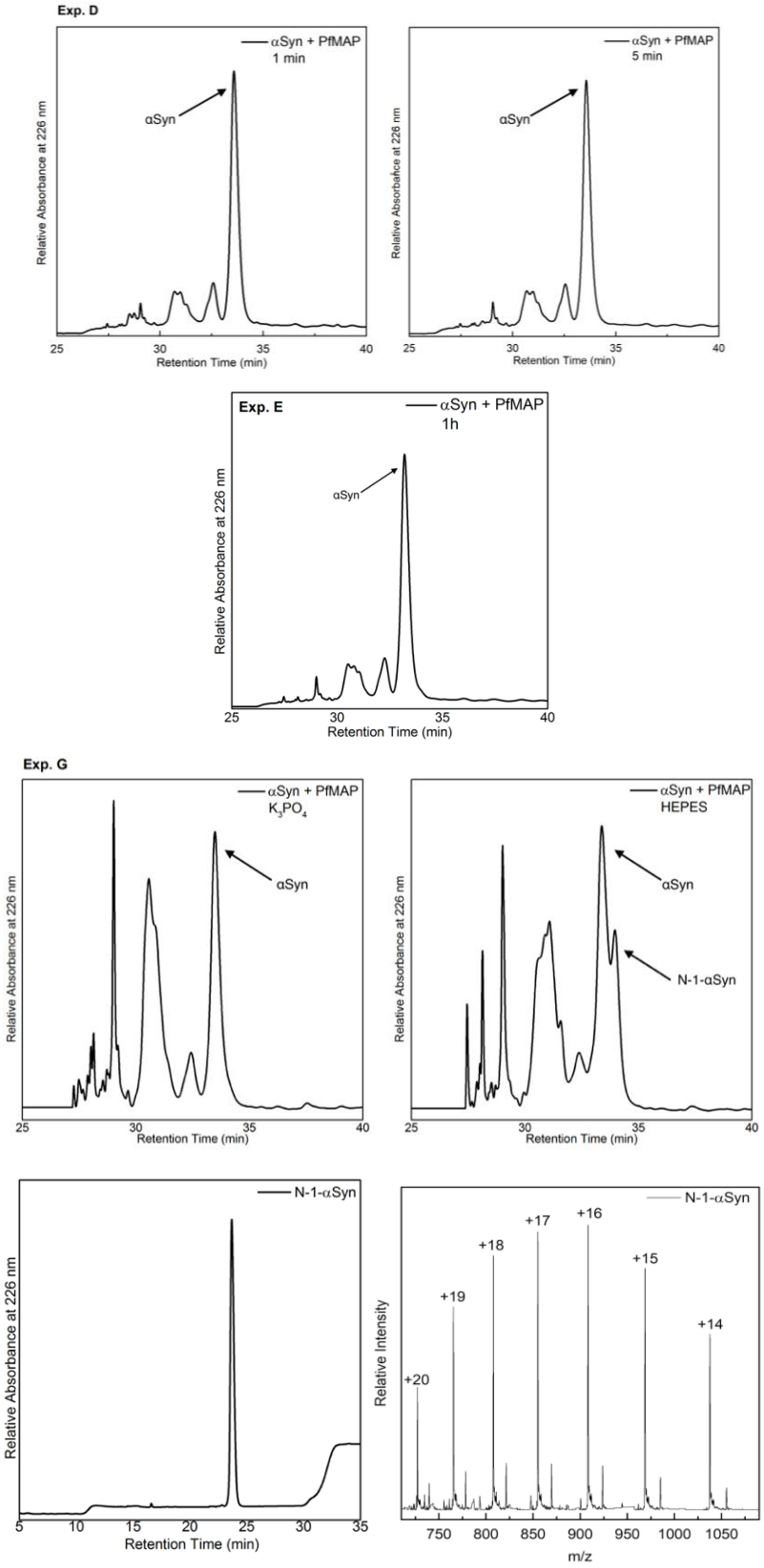

Fig. 3.3. *Results from the set-up of the production method, identification and characterization of N-1-αSyn*. On the top, the chromatograms of exp. D & E show no reaction ocurring as the only band present is the one of αSyn. At the bottom, in the results of exp. G, the pick labelled as N-1-αSyn when using HEPES buffer was confirmed to be the αSyn lacking the N-terminal Met by the MS analysis shown below. Additionally, the RP-HPLC characterization shows N-1-αSyn eluting at 23.7 min. The complete conditions of the production reactions are found in table 3.2.

After confirming that the objective was accomplished, further conditions were tested to improve the yield of the reaction and to reduce the amount of enzyme employed. Lower m/m ratios were used (exp. H), as well as a second addition of enzyme to the reaction after an overnight incubation (Fig. 3.4, exp. I). Another buffer (*RapiGest*^{TM}) was employed to try to increase the stability of the αSyn while incubation, and therefore, the production yield. However, the results were negative: in this case there was not any N-1-αSyn produced (Fig. 3.4, exp. J).

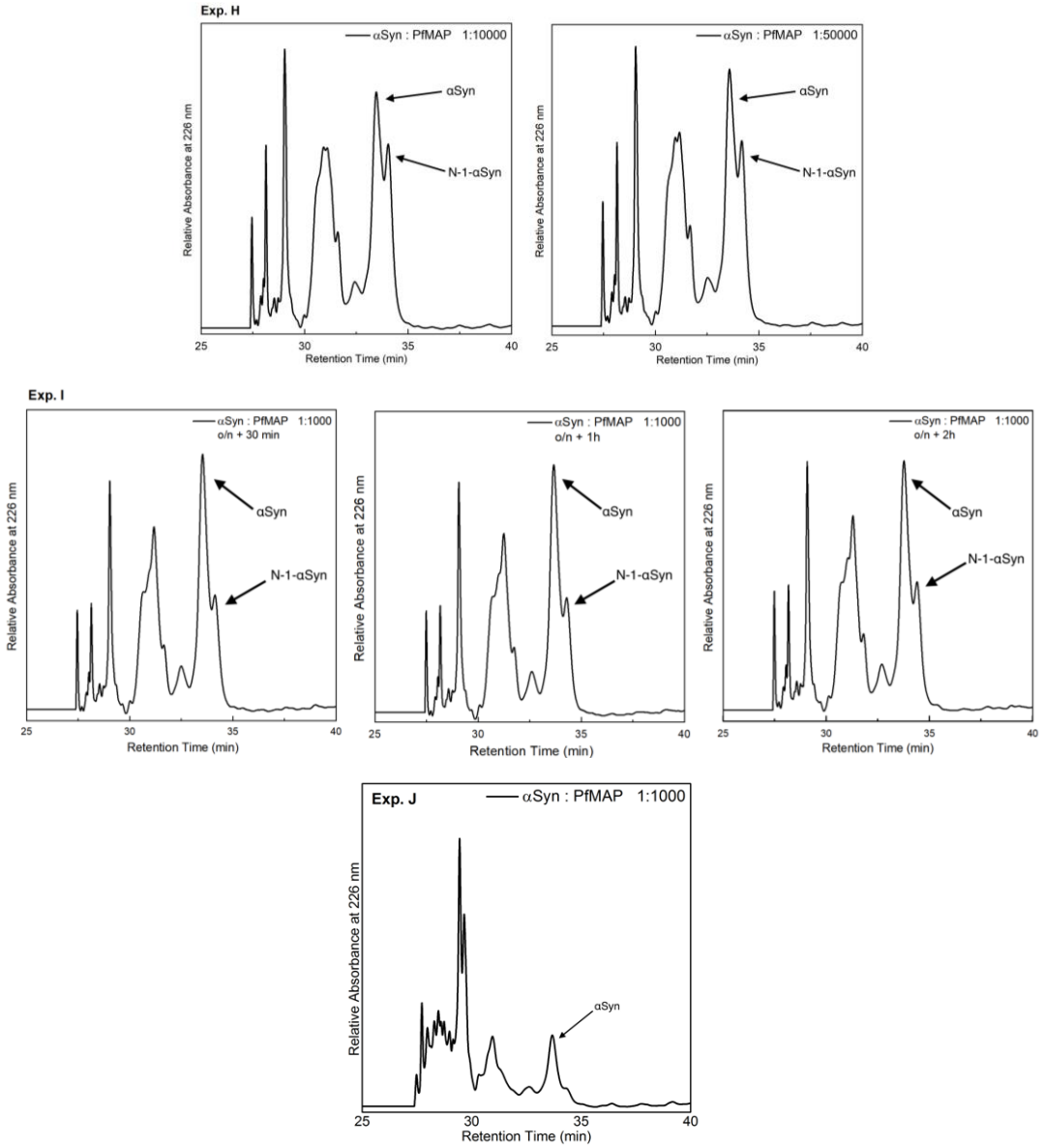

Fig. 3.4. *Results from the set-up of the production method of N-1-αSyn.* The chromatograms of exp. H (on the top) and I (in the middle) show that the reactions are successful in all their different conditions, which are detailed in table 3.2. On the contrary, exp. J results (at the bottom) show no reaction ocurring in addition to a higher degradation of the protein when using RapiGest™ buffer.

Considering all the experiments performed and their results (Table 3.2), the best reaction conditions for the production of the N-1-αSyn were set as explained in table 3.1, which were employed in exp. K & L (Fig. 3.5) to make sure that the reaction could be scaled-up.

Table 3.1. *Optimum reaction conditions for the N-1-αSyn production after all the method set-up*.

Buffer	T (ºC)	Enzyme Inhibition	MAP:αSyn	Time
HEPES	37	EDTA 3 mM	1:50000	o/n

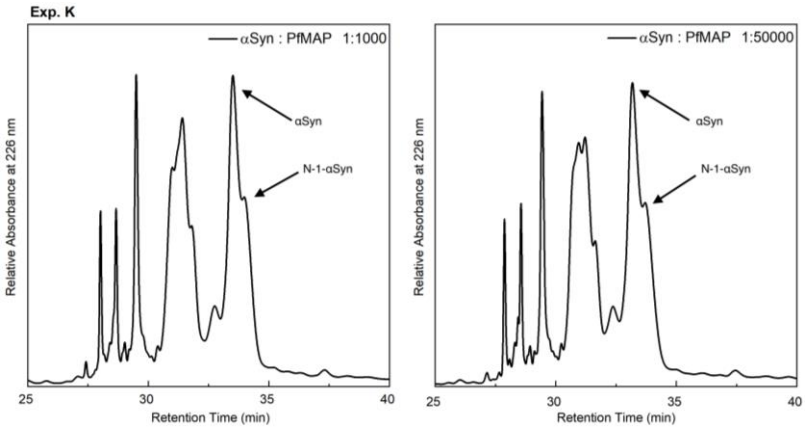

Fig. 3.5. *Results from the set-up of the production method of N-1-αSyn.* Exp. K is the last one performed before the protein production. For it, 500 µg of αSyn were used in two different MAP:αSyn ratios, 1:1000 and 1:50000, to be sure that what succeeded with a much lower amount of protein could be scaled-up. Both conditions succeeded, therefore, the lower amount of enzyme was selected as the optimum one, because of saving reasons.

Table 3.2. All the experiments performed for the N-1-αSyn production and their specific conditions and results.

Exp.	αSyn (µg) per condition	αSyn (µg/µL)	Buffer	T (ºC)	Enzyme inhibition	Analysis	MAP:αSyn	Time	Result
A	15	1	HEPES	37	2 min in boiling water	MS	1:1000	1h	_*
								2h	_*
								3h	_*
								o/n	_*
B	15	1	HEPES	37	2 min in boiling water	MS	1:10000	1h	_*
								2h	_*
								3h	_*
								o/n	_*
C	30	1	HEPES	37	2 min in boiling water	MS	1:50000	1 min	_*
								5 min	_*
								10 min	_*
								1h	_*
								3h	_*
D	30	1	K_3PO_4	37	EDTA 3 mM	HPLC	1:50000	1 min	_
								5 min	_
								10 min	_
								1 h	_
E	30	1	K_3PO_4	37	EDTA 3 mM	HPLC	1:1000	1 min	_
								5 min	_
								10 min	_
								1h	_
F	30	1	HEPES	30	EDTA 3 mM	HPLC	1:1000	1h	_
							1:10000	1h	_
							1:50000	1h	_

G	20	1	K_3PO_4	37	EDTA 3 mM	HPLC	1:1000	o/n	_
			HEPES	37	EDTA 3 mM	HPLC	1:1000	o/n	+
H	20	1	HEPES	37	EDTA 3 mM	HPLC	1:10000	o/n	+
							1:50000	o/n	+
I	20	2	HEPES	37	EDTA 3 mM	HPLC	1:50000	o/n + 1h	+
								o/n + 3h	+
								o/n + 6h	+
							1:1000	o/n + 30 min	+
								o/n + 1h	+
								o/n + 2h	+
J	30	2	RapiGest	37	EDTA 3 mM	HPLC	1:1000	1h	_
								3h	_
								6h	_
								o/n	_
							1:50000	1h	_
								3h	_
								6h	_
								o/n	_
K	500	2	HEPES	37	EDTA 3 mM	HPLC	1:1000	o/n	+
							1:50000	o/n	+
L	500 (x3)	2	HEPES	37	EDTA 3 mM	HPLC	1:50000	o/n	+

* αSyn completely degraded.

Liposome characterization

The DLS analyses showed that the liposomes produced were of high quality (Fig. 3.6). The polydispersity index was 0.061, which is between 0.05 and 0.7, meaning that the sample is nearly monodispersed. The average diameter was 137 nm, the width was 36 nm and the Z-Average was 128 d.nm.

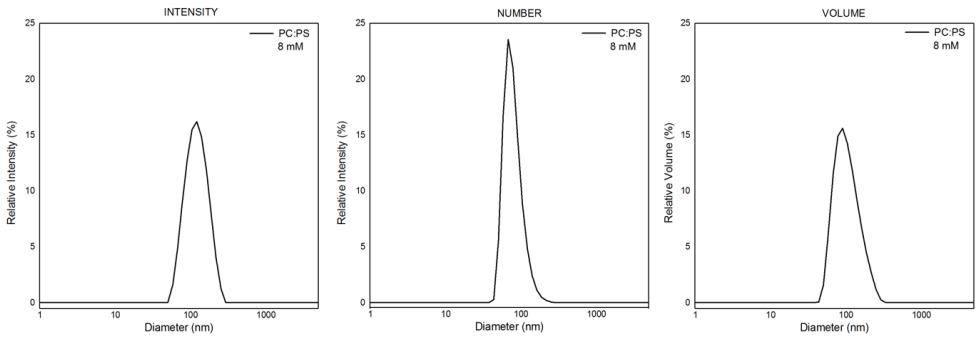

Fig. 3.6. *DLS analyses of the liposomes produced*. The existence of a single pick in the three chromatograms confirms that the production was of high quality and monodispersed.

4.1.3. Oxidation of α-Synuclein

αSynOx was produced starting from freshly-solubilized αSyn following a protein oxidation protocol; briefly, the protein was treated with 4% H_2O_2 and left for 20 min to complete the reaction. The aim of the experiment was to oxidize all four methionine residues of αSyn. The product of the

oxidation was purified by RP-HPLC and the corresponding pick was analyzed by MS, which confirmed the oxidation of the four Met residues (Fig. 3.7).

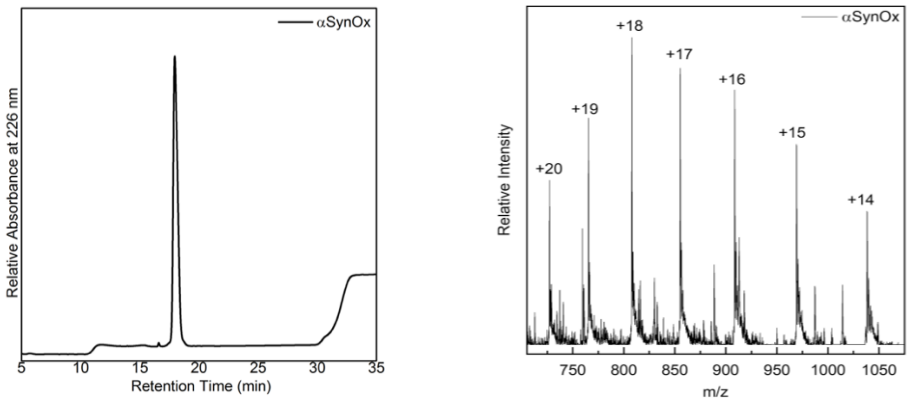

Fig. 3.7. *Idetification and characterization of αSynOx*. The chromatogram on the left shows the RP-HPLC analysis with the αSynOx eluting at 18 min. The one on the right shows the MS analysis.

4.2. Comparison of α-Synuclein, N-1-α-Synuclein and oxidized α-Synuclein

In order to accomplish reproducibility enough to be able to extract conclusions from the comparison of the analyses from the three species, they were always performed with two previous blanks: one without any sample injected, and another one with pure αSyn.

4.2.1. Chemical comparison: RP-HPLC & MS

To chemically compare the three species, they were subjected to a round of RP-HPLC analyses with the same gradient. The protein material corresponding to the isolated fractions was then analyzed by means of MS. Clear differences in the retention times were observed (Fig. 3.8). While αSynOx showed a retention time of 18.0 min, αSyn and N-1-αSyn eluted later at 20.8 min and 23.7 min, respectively. As an increasingly hydrophobic gradient was used, lower retention times represent higher hydrophilicity, while higher retention times mean higher hydrophobicity.

αSynOx presented a higher hydrophilic character compared to αSyn, the oxidation of the protein adds one oxygen atom to each of the four Met residues; overall, the chemical modification decreases αSynOx affinity for the stationary phase, and increases the protein affinity for the mobile phase. On the contrary, αSyn lacks those oxygen atoms, presenting a higher hydrophobicity and therefore eluting later. Interestingly, N-1-αSyn eluted even later than αSyn. The removal of the N-terminal Met made the second amino acid able to interact with the environment. The second residue is an Asp, which is more hydrophilic than Met. Nevertheless, the RP-HPLC run is conducted at acidic pH, where Asp is protonated. Therefore, the Asp in the second position passed from being deprotonated in the αSyn polypeptide chain, to being exposed to the acidic environment and therefore protonated in the N-1-αSyn one. Overall, this conferred hydrophobicity to N-1-αSyn.

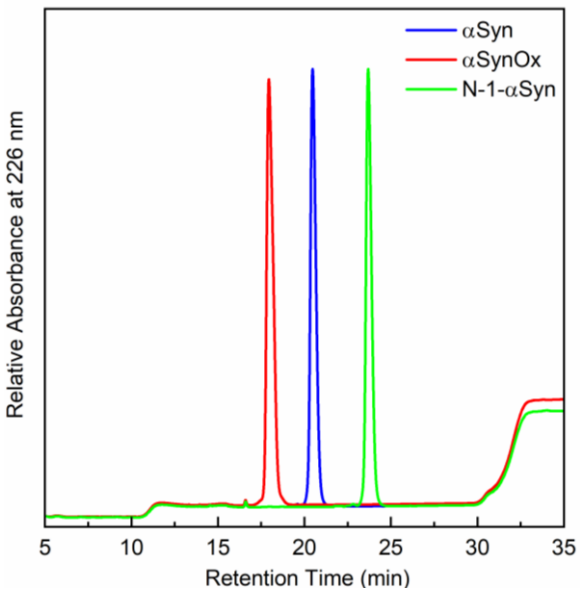

Fig. 3.8. *Comparison of the RP-HPLC characterization of the three proteins*. αSyn, αSynOx and N-1-αSyn show different retention times: 20.8, 18 and 23.7 min, respectively; and therefore, different hydrophobic properties, being αSynOx the one with the lowest hydrophobicity and N-1-αSyn the one with the highest.

The MS analyses confirm the presence of the MW shift associated with the oxidation of the four Met residues and the processing of the N-terminal one (Fig. 3.9). The calculated MW for αSyn is 14458.7 Da, which corresponds to its theoretical MW (14460.2 Da). On the one hand, the calculated MW for αSynOx is 14522.9 Da; an increment of +64.2 Da from αSyn, corresponding to four oxygen atoms of 16 Da, one from each Met oxidation. The calculated MW for N-1-αSyn is 14329.0 Da as expected and it corresponds to the lack of the Met residue (131.2 Da).

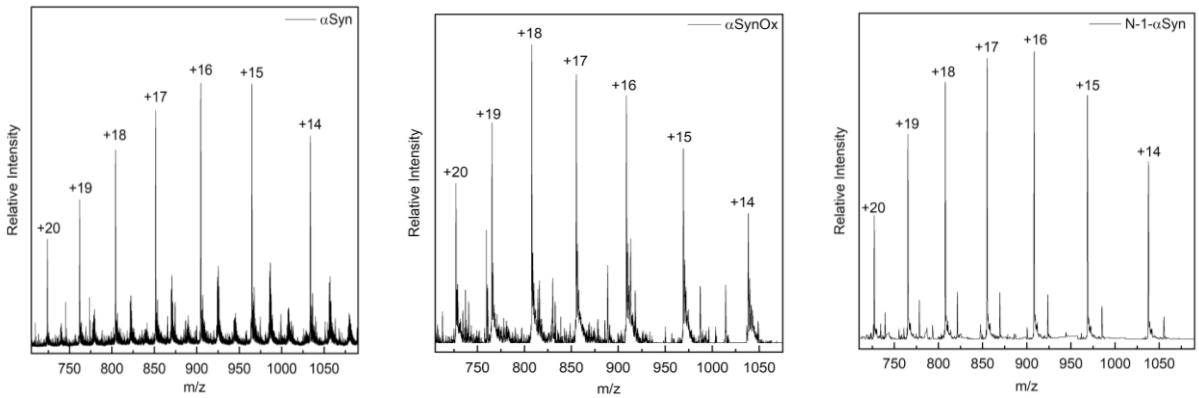

Fig. 3.9. *Comparison of the MS characterization of αSyn, αSynOx and N-1-αSyn.*

4.2.2. Conformational comparison: SEC & CD

With the aim of clarifying if the oxidation influences the conformational state of αSynOx, and if the processing of the N-terminal Met residue influences the one of N-1-αSyn, both SEC and CD analyses took place. All samples were analyzed after solubilization from lyophilized powder state,

filtration with a 0.22 µm filter, UV quantification to ensure equal concentrations, and, in the case of the SEC analyses, also centrifugation to avoid ruining the column with possibly present large aggregates or other insoluble particles.

The SEC chromatograms show that αSyn elute at 14.1 mL (Fig. 3.11). Considering the calibration curve, it corresponds to a protein of 62 kDa. In fact, in the SEC analyses, αSyn behaves as a protein with more than four times its actual MW because of its native random conformation nature as IDP. This accelerates the passage of both species through the column due to the fact that the proteins cannot easily enter in the size-exclusion pores, just as it occurs in big proteins. Interestingly, αSynOx elutes exactly at the same elution volume as αSyn, behaving as well as a 62 kDa protein. Taking this into consideration, it seems that the oxidation of the four Met residues does not change the random character of the protein, however, this has to be confirmed by CD analysis. Differently, N-1-αSyn does show a considerable variation on the elution volume. In this case it elutes at 15.6 mL, corresponding to a protein with a MW of 30.2 kDa, which is less than the half of the 62kDa of the αSyn SEC-apparent MW, but still the double of its actual MW. Before confirmation by CD, it could be hypothesized that the N-1-αSyn still keeps the IDP native disordered structure that prevents it from entering smaller column pores and consequently eluting earlier. However, this unstructured conformation seems to be much more compacted, perhaps due to the increase in hydrophobicity observed in RP-HPLC, as the apparent MW is half the one of WT-αSyn.

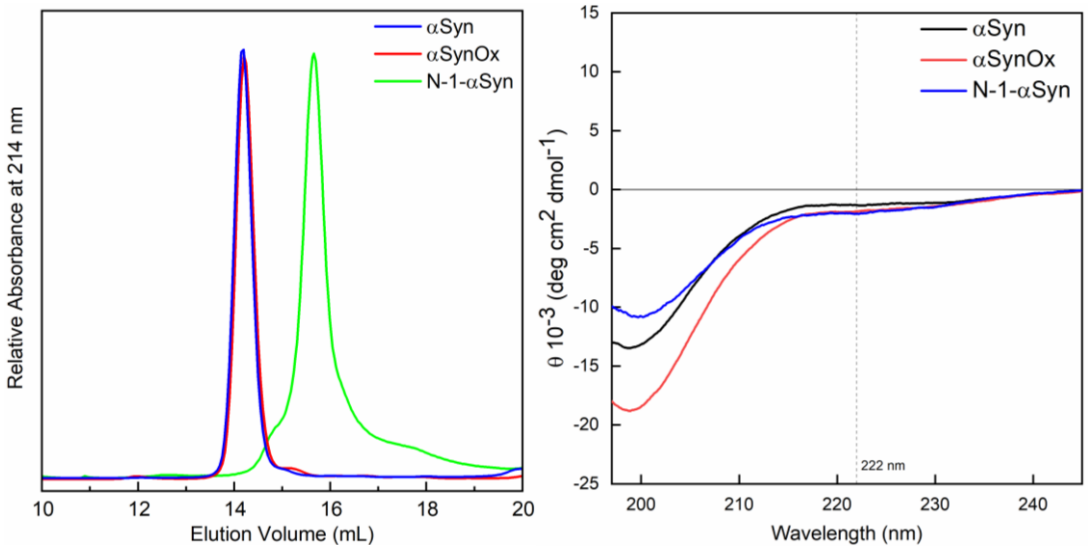

Fig. 3.10. *Comparison of the SEC (on the left) and the CD (on the right) characterization of αSyn, αSynOx and N-1-αSyn*. The three species show very similar spectra characteristic of disordered structures. Moreover, N-1-αSyn shows a much smaller SEC-apparent MW (eluting at 15.6 mL) compared to αSyn and αSynOx, which elute much earlier (14.1 mL).

In order to confirm the previously mentioned hypothesis about the random character in the structure of the three species, they underwent CD evaluation. As can be appreciated on figure 3.10, the three species under study do show intrinsically-disordered nature. Therefore, it can be stated that neither the oxidation of the four Met residues nor the processing of the N-terminal Met, modify the type of structure of the αSyn in these conditions. However, combining the results of SEC and CD, it could be as well stated that N-1-αSyn shows a much more compact random structure compared to αSyn and αSynOx.

4.2.3. Interaction with micelles and liposomes: CD

Provided that the proteins under investigation were characterized in solution, another logical step was to test the behavior of αSyn, αSynOx and N-1-αSyn in the presence of SDS micelles and liposomes. SDS is an amphiphilic surfactant that forms micelles in aqueous medium above its critical micellar concentration (CMC). The hydrophilic, negatively-charged head groups associate with water while the hydrophobic tails aggregate inside the micelle core. SDS was chosen to perform an initial characterization of the three species in the presence of a smaller and simpler system, before moving to a more complex liposomal system. Far-UV CD analyses were performed with an SDS concentration of 10 mM, which is above its CMC (8.5 mM).

The comparison of the far-UV CD spectra of the three proteins with and without interactor is shown in figure 3.11. As previously stated, αSyn, αSynOx and N-1-αSyn show a random coil structure without the presence of any interactor. However, in the presence of SDS micelles, the three of them present a clear α-helical structure. Additionally, the three spectra are separated only by a small difference that most surely come from experimental errors on the protein concentration, meaning that the amount of α-helix in the three samples is basically the same, therefore, it could be stated that the three proteins present an equal interaction with the SDS micelles. That is, neither the oxidation of the four Met residues nor the processing of the N-terminal Met have any effect on the interaction of the αSyn with the SDS micelles.

Since it is known that αSyn interacts with lipid membranes and after having achieved the results of the interaction with the simpler SDS micelles. The same study was performed with more complex liposomes, which were self-produced with a high quality as previously shown in figure 3.6. The formulation PC:PS 1:1 was chosen because it showed to be the best option in previous experiments performed in the same laboratory (data to be published protected by copy right). Phosphatidylcholine (PC) is the most abundant phospholipid in the outer part of the biological membranes and phosphatidylserine (PS) is the major acidic phospholipid class found on cellular membranes; its

negatively charged head group allows interaction with αSyn. The m/m ratio protein:liposomes chosen was 1:10 as an initial point for the characterization of the interaction.

The comparison between the three species with and without interactor is shown in figure 3.11. A clear α-helical structure is shown again in the three cases. However, the minimum at 222 nm of αSynOx is higher, therefore, the amount of α-helix formed is lower than in the other two cases. Consequently, the oxidation of the four Met residues does modify the interaction between the protein and the liposomes at a 1:10 ratio. According to literature, the folding of αSyn to α-helical structure when interacting with the cellular membrane could start with the first interaction of the N-terminal Met with the lipid bilayer. Then, the rest of the protein would follow, folding in α-helix all the way through the NAC domain, leaving the C-terminal tail unfolded. Following this hypothesis, the oxidation of the Met residues would hinder the starting anchoring interaction which would drive the folding of the native non-oxidized αSyn, making αSynOx able to acquire structure only in the central part of the N-terminal domain. However, the spectra of αSyn and N-1-αSyn are identical, meaning that the processing of the N-terminal Met does not modify the interaction of the protein with the liposomes in a 1:10 ratio. Therefore, the N-terminal Met seems not to be essential for the α-helix formation, which rejects the previously mentioned hypothesis found in the literature. This way, it seems that the reduction on the interaction of the αSynOx with the hydrophobic surface of the liposomes is due to the higher hydrophilicity that the MetOx residues give to the N-terminus (positions 1 and 5) and the C-terminus (positions 116 and 127), letting open the possibility that the central NAC domain still forms the α-helix. Still, it could also be that the α-helix shown comes from the non-oxidized αSyn that may still be present in the sample from the very beginning or because of the reduction of the protein during the analyses period.

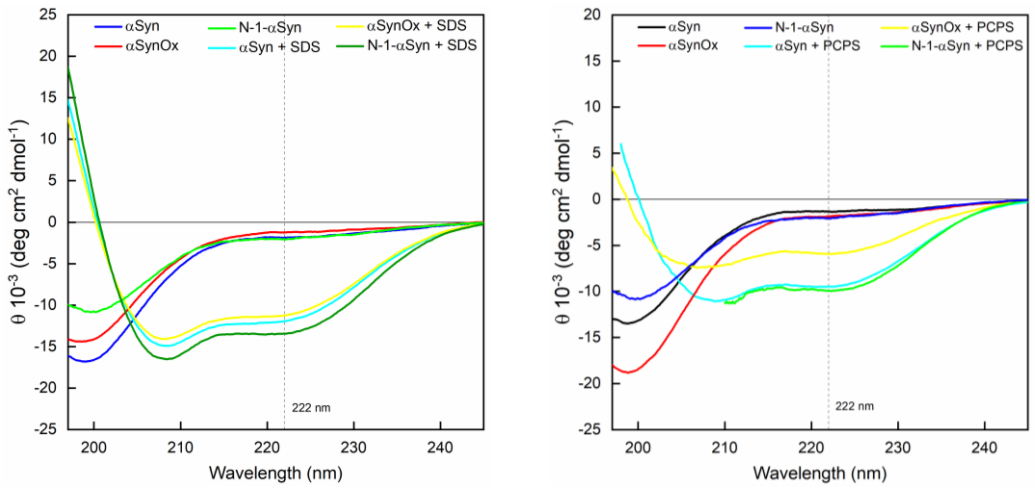

Fig. 3.11. *Comparison of the CD characterization of αSyn, αSynOx and N-1-αSyn with and without the presence of SDS micelles (on the left) and liposomes 1:10 (on the right).* In the presence of SDS micelles, the three proteins fold into an α-helical structure with the same spectrum form. In the presence of liposomes, they also fold into an α-helical structure, but they do it differently: αSynOx presents a higher minimum at 222 nm meaning that the amount of secondary structure formed is lower than in the case of αSyn and N-1-αSyn.

5. Conclusions

The optimum reaction conditions for the N-1-αSyn production still have a very low yield because of the unfolding nature of αSyn, which makes difficult to find an equilibrium in the conditions so that the protease cleaves the first residue without losing the specificity.

Chemically, αSynOx show higher hydrophilicity due to the presence of four additional oxygen atoms in the polypeptide chain. On the contrary, N-1-αSyn show higher hydrophobicity, likely conferred by the protonation of the residue in the second position (Asp) now exposed to the RP-HPLC acidic environment.

Conformationally, αSynOx and N-1-αSyn show random structures as αSyn does, however, the random structure of N-1-αSyn seems to be more compact compared to the others, possibly due to its higher hydrophobicity.

When interacting with liposomes, αSynOx show a lower amount of α-helical structure compared to the others due to its higher hydrophilicity.

N-1-αSyn forms α-helix in the same proportion that αSyn does, therefore, the hypothesis stating that the N-terminal Met is crutial for the αSyn anchoring to membranes is wrong.

6. Bibliography

- AHN, M.; KIM, S.; KANG, M.; RYU, Y.; KIM, T.D. Chaperone-like activities of α-synuclein: α-Synuclein assists enzyme activities of esterases. *Biochemical and Biophysical Research Communications* **2006**, *346*, *4*, 1142-1149.
- AKBARZADEH, A.; REZAEI-SADABADY, R.; DAVARAN, S.; JOO, S.W.; ZARGHAMI, N.; HANIFEHPOUR, Y.; SAMIEI, M.; KOUHI, M.; NEJATI-KOSHKI, K. Liposome: Classification, preparation, and applications. *Nanoscale Res. Lett*. **2013**, *8*, 110.
- AMARNATH, S.; SHARMA, U.S. Liposomes in drug delivery: progress and limitations. *Int J Pharm* **1997**, *154*, 123–140.
- AMERSHAM BIOSCIENCES. *Ion Exchange Chromatography Principles and Methods. General Electric Company,* 2004.
- ANTONNY, B. Mechanisms of membrane curvature sensing. *Annu. Rev. Biochem* **2011**, *80*, 101–123.
- BEN-BASSAT, A.; BAUER, K.; CHANG, S.Y.; MYAMBO, K.; BOOSMAN, A.; CHANG, S. Processing of the initiation methionine from proteins: properties of the Escherichia coli methionine aminopeptidase and its gene structure. *J Bacteriol* **1987**, *169(2)*, 751-7.
- BERNE, B.J.; PECORA, R. *Dynamic light scattering: with applications to chemistry, biology, and physics*. John Wiley & Sons, Inc, New York, USA, 1976.
- BODNER, C.R.; DOBSON, C.M.; BAX, A. Multiple tight phospholipid-binding modes of α-synuclein revealed by solution NMR spectroscopy. *J. Mol. Biol* **2009**, *390*, 775–790.
- BODNER, C.R.; MALTSEV, A.S.; DOBSON, C.M.; BAX, A. Differential phospholipid binding of α-synuclein variants implicated in Parkinson's disease revealed by solution NMR spectroscopy. *Biochemistry* **2010**, *49*, 862–871.
- BOOSMAN, A.; CHANG, S. Processing of the initiation methionine from proteins: properties of the Escherichia coli methionine aminopeptidase and its gene structure. *J Bacteriol*. **1987**, *169(2)*, 751-7.
- BURRÉ, J.; SHARMA, M.; SÜDHOF, T. C. Cell biology and pathophysiology of α-synuclein. *Cold Spring Harb. Perspect. Med*. **2018**, *8*, a024091.
- BURRÉ, J.; SHARMA, M.; TSETSENIS, T.; BUCHMAN, V.; ETHERTON, M.R.; SÜDHOF, T.C. α- Synuclein promotes SNARE-complex assembly in vivo and in vitro. *Science* **2010**, *329*, 1663– 1667.
- CHANDRA, S.; GALLARDO, G.; FERNANDEZ-CHACON, R.; SCHLUTER, O.M.; SÜDHOF, T.C. α- Synuclein cooperates with CSPα in preventing neurodegeneration. *Cell* **2005**, *123*, 383–396.
- CHEN, H.; RITZ, B. *The Search for Environmental Causes of Parkinson's Disease: Moving Forward*. J. Parkinsons Dis., 2018.
- CHOLAK, E.; BUGGE, K.; KHONDKER, A.; GAUGER, K.; PEDRAZ-CUESTA, E.; PEDERSEN, M.E.; BUCCIARELLI, S.; VESTERGAARD, B.; PEDERSEN, S.F.; RHEINSTÄDTER, M.C.; LANGKILDE, A.E.; KRAGELUND, B.B. Avidity within the N-terminal anchor drives α-synuclein membrane interaction and insertion. *FASEB J* **2020**, *34(6)*, 7462-7482.
- CHRAI, S.S.; MURARI, R.; IMRAN, A. Liposomes: a review. *Bio Pharm* **2001**, *14(11)*, 10–14.
- CHU, Y.; KORDOWER, J.H. Age-associated increases of αsynuclein in monkeys and humans are associated with nigrostriatal dopamine depletion: Is this the target for Parkinson's disease? *Neurobiol Dis* **2007**, *25*, 134–149.
- CLAYTON, D.F.; GEORGE, J.M. The synucleins: A family of proteins involved in synaptic function, plasticity, neurodegeneration and disease. *Trends Neurosci* **1998**, *21*, 249– 254.

- CONWAY, K.A.; HARPER, J.D.; LANSBURY, P.T. Accelerated in vitro fibril formation by a mutant α-synuclein linked to early-onset Parkinson disease. *Nat Med* **1998**, *4*, 1318–1320.
- CONWAY, K.A.; LEE, S.J.;ROCHET, J.C.; DING, T.T.; HARPER, J.D,.; WILLIAMSON, R.E.; LANSBURY, P.T. JR. Accelerated oligomerization by Parkinson's disease linked α-synuclein mutants. *Ann NY Acad Sci* **2000**, *920*, 42–45.
- COOPER, A.A.; GITLER, A.D.; CASHIKAR, A.; HAYNES, C.M.; HILL, K.J.; BHULLAR, B.; LIU, K.; XU, K.; STRATHEARN, K.E.; LIU, F.; *et al*. α-Synuclein blocks ER-Golgi traffic and Rab1 rescues neuron loss in Parkinson's models. *Science* **2006**, *313*, 324–328.
- DA COSTA, C.A.; ANCOLIO, K.; CHECLER, F. Wild-type but not Parkinson's disease-related Ala53 Thr mutant α-synuclein protects neuronal cells from apoptotic stimuli. *J Biol Chem* **2000**, *275*, 24065–24069.
- DALBØGE, H.; BAYNE, S.; PEDERSEN, J. In vivo processing of N-terminal methionine in *E. coli*. *FEBS Lett* **1990**, *266(1-2)*, 1-3.
- DAS, T.; ELIEZER, D. Membrane interactions of intrinsically disordered proteins: The example of alpha-synuclein. *Biochim Biophys Acta Proteins Proteom* **2019**, *1867(10)*, 879-889.
- DAVIDSON, W.S.; JONAS, A.; CLAYTON, D.F.; GEORGE, J.M. Stabilization of α-synuclein secondary structure upon binding to synthetic membranes. *J Biol Chem* **1998**, *273*, 9443– 9449.
- DE HOFFMANN, E.; STROOBANT, V. *Mass Spectrometry: Principles and Applications, 3rd Edition,* 2007.
- DEMAAGD, G.; PHILIP, A. *Parkinson's Disease and Its Management: Part 1: Disease Entity, Risk Factors, Pathophysiology, Clinical Presentation, and Diagnosis.* P & T, 2015.
- DIKIY, I.; ELIEZER, D. N-terminal Acetylation Stabilizes N-terminal Helicity in Lipid- and Micelle-bound α-Synuclein and Increases Its Affinity for Physiological Membranes. *Journal of Biological Chemistry* **2014**, *289*, *6*, 3652-3665.
- DING, T.T.; LEE, S.J.; ROCHET, J.C.; LANSBURY, P.T. JR. Annular α-synuclein protofibrils are produced when spherical protofibrils are incubated in solution or bound to brain- derived membranes. *Biochemistry* **2002**, *41*, 10209–10217.
- EL-AGNAF, O.M.; JAKES, R.; CURRAN, M.D.; WALLACE, A. Effects of the mutations Ala30 to Pro and Ala53 to Thr on the physical and morphological properties of α-synuclein protein implicated in Parkinson's disease. *FEBS Lett* **1998**, *440*, 67–70.
- ELIEZER, D.; KUTLUAY, E.; BUSSELL, R.; JR BROWNE, G. Conformational properties of a- synuclein in its free and lipidassociated states. *J Mol Biol* **2001**, *307*, 1061–1073.
- ELSWORTH, J.D. *Parkinson's disease treatment: past, present, and future.* J. Neural Transm, 2020.
- EMAMZADEH, F.N. *Alpha-synuclein structure, functions, and interactions.* J. Res. Med. Sci*,* 2016.
- ESPOSITO, A.; DOHM, C.P.; KERMER, P.; BÄHR, M.; WOUTERS, F.S. α-Synuclein and its disease-related mutants interact differentially with the microtubule protein tau and associate with the actin cytoskeleton. *Neurobiology of Disease* **2007**, *26*, *3*, 521-531.
- FARES, M.B.; AIT-BOUZIAD, N.; DIKIY, I.; MBEFO, M.K.; JOVIČIĆ, A.; KIELY, A.; HOLTON, J.L.; LEE, S.J; GITLER, A.D; ELIEZER, D.; LASHUEL, H.A. The novel Parkinson's disease linked mutation G51D attenuates in vitro aggregation and membrane binding of α-synuclein, and enhances its secretion and nuclear localization in cells. *Hum. Mol. Genet*. **2014**, *23*, 4491–4509.
- FORTIN, D.L.; NEMANI, V.M.; VOGLMAIER, S.M.; ANTHONY, M.D.; RYAN, T.A.; EDWARDS, R.H. Neural activity controls the synaptic accumulation of α-synuclein. *JNeurosci* **2005**, *25*, 10913– 10921.

- FREDENBURG, R.A.; ROSPIGLIOSI, C.; MERAY, R.K.; KESSLER, J.C.; LASHUEL, H.A.; ELIEZER, D.; LANSBURY, P.T. JR. The impact of the E46K mutation on the properties of α- synuclein in its monomeric and oligomeric states. *Biochemistry* **2007**, *46*, 7107–7118.
- FROTTIN, F.; MARTINEZ, A.; PEYNOT, P.; MITRA, S.; HOLZ, R.C.; GIGLIONE, C.; MEINNEL, T. The proteomics of N-terminal methionine cleavage. *Mol Cell Proteomics* **2006**, *5(12)*, 2336-49.
- FUSCO, G.; DE SIMONE, A.; GOPINATH, T.; *et al*. Direct observation of the three regions in α- synuclein that determine its membrane-bound behaviour. *Nat Commun* **2014**, *5*, 1-8.
- FUSCO. G.; PAPE, T.; STEPHENS, A.D.: MAHOU, P.; COSTA, A.R.; KAMINSKI, C.F.; KAMINSKI SCHIERLE, G.S.; VENDRUSCOLO, M.; VEGLIA, G.; DOBSON, C.M.; DE SIMONE, A. Structural basis of synaptic vesicle assembly promoted by α-synuclein. *Nat. Commun* **2016** *7*, 12563.
- GLASER, C.B.; YAMIN, G.; UVERSKY, V.N.; FINK, A.L. Methionine oxidation, alpha-synuclein and Parkinson's disease. *Biochim Biophys Acta* **2005**, *1703(2)*, 157-69.
- GLISH, G.L.; VACHET, R.W. The basics of mass spectrometry in the twenty-first century. *Nat. Rev. Drug Discov.* **2003**, 2, 140.
- GORBATYUK, O.S.; LI, S.; NGUYEN, F.N.; MANFREDSSON, F.P.; KONDRIKOVA, G.; SULLIVAN, L.F.; MEYERS, C.; CHEN, W.; MANDEL, R.J.; MUZYCZKA, N. α-Synuclein expression in rat substantia nigra suppresses phospholipase D2 toxicity and nigral neurodegeneration. *Mol Ther* **2010**, *18*, 1758–1768.
- GOSAVI, N.; LEE, H.J.; LEE, J.S.; PATEL, S.; LEE, S.J. Golgi fragmentation occurs in the cells with prefibrillar α-synuclein aggregates and precedes the formation of fibrillar inclusion. *J Biol Chem* **2002**, *277*, 48984–48992.
- GREENBAUM, E.A.; GRAVES, C.L.; MISHIZEN-EBERZ, A.J.; LUPOLI, M.A.; LYNCH, D.R.; ENGLANDER, S.W.; AXELSEN, P.H.; GIASSON, B.I. The E46K mutation in α-synuclein increases amyloid fibril formation. *J Biol Chem* **2005**, *280*, 7800–7807.
- GRETEN-HARRISON, B.; POLYDORO, M.; MORIMOTO-TOMITA, M.; DIAO, L.; WILLIAMS, A.M.; NIE, E.H.; MAKANI, S.; TIAN, N.; CASTILLO, P.E.; BUCHMAN, V.L.; et al. αβγ-Synuclein triple knockout mice reveal age-dependent neuronal dysfunction. *Proc Natl Acad Sci* **2010**, *107*, 19573–19578.
- GRIFFITHS, A.J.F.; GELBART, W.M. *Modern Genetic Analysis*. New York: W. H. Freeman, 1999.
- GUO, J.T.; CHEN, A.Q.; KONG, Q.; ZHU, H.; MA, C.M.; QIN, C. Inhibition of vesicular monoamine transporter-2 activity in α-synuclein stably transfected SH-SY5Y cells. *Cell Mol Neurobiol* **2008**, *28*, 35–47.
- HAYES, M.T. Parkinson's disease and Parkinsonism. *Am. J. Med*. **2019**, 802-807.
- HIREL, P.H.; SCHMITTER, M.J.; DESSEN, P.; FAYAT, G.; BLANQUET, S. Extent of N-terminal methionine excision from Escherichia coli proteins is governed by the side-chain length of the penultimate amino acid. *Proc Natl Acad Sci U S A* **1989**, *86(21)*, 8247-51.
- HOYER, W.; ANTONY, T.; CHERNY, D.; HEIM, G.; JOVIN, T.M.; SUBRAMANIAM, V. Dependence of α-Synuclein Aggregate Morphology on Solution Conditions. *Journal of Molecular Biology* **2002**, *322*, *2*, 383-393.
- HURLEY, J.H. Membrane binding domains. *Biochim. Biophys. Acta - Mol. Cell Biol. Lipids* **2006**, *1761*, 805–811.
- ISBIR ,T.; KIRAC, D.; DEMIRCAN, B.; DALAN, B. *Gel Electrophoresis.* Brenner's Encyclopedia of Genetics (Second Edition). Academic Press 2013; pp 165-167.
- JAO, C.C.; HEGDE, B.G.; CHEN, J.; HAWORTH, I.S.; LANGEN, R. Structure of membranebound alpha-synuclein from site-directed spin labeling and computational refinement. *Proc. Natl. Acad. Sci. U. S. A.* **2008**, *105*, 19666–19671.

- JIANG, Z.; DE MESSIERES, M.; LEE, J.C. Membrane remodeling by α-synuclein and effects on amyloid formation. *J. Am. Chem. Soc* **2013**, *135*, 15970–15973.
- JO, E.; MCLAURIN, J.; YIP, C.M.; ST GEORGE-HYSLOP, P.; FRASER, P.E. α-Synuclein membrane interactions and lipid specificity. *J Biol Chem* **2000**, *275*, 34328–34334.
- KEBARLE, P.; VERKERK, U.H. Electrospray: From Ions in Solution to Ions in the Gas Phase, What We Know Now. *Mass Spectrom Rev.* **2009**, *28(6)*, 898–917.
- KELLY, S.M.; PRICE, N.C. The application of circular dichroism to studies of protein folding and unfolding. *Biochim. Biophys. Acta* **1997**, *1338*, 161–185.
- KIM, T.D.; CHOI, E.; RHIM, H.; PAIK, S.R.; YANG, C.H. α-Synuclein has structural and functional similarities to small heat shock proteins. *Biochemical and Biophysical Research Communications* **2004**, *324, 4*, 1352-1359.
- LAI, Y.; KIM, S.; VARKEY, J.; LOU, X.; SONG, J.K.; DIAO, J.; LANGEN, R.; SHIN, Y.K. Nonaggregated α-synuclein influences SNARE-dependent vesicle docking via membrane binding. *Biochemistry* **2014**, *53*, 3889–3896.
- LANGSTON, J.W. The MPTP Story. *J. Parkinsons Dis*. **2017**, *7*.
- LAPINSKI, M.M.; CASTRO-FORERO, A.; GREINER, A.J.; OFOLI, R.Y.; BLANCHARD, G.J. Comparison of liposomes formed by sonication and extrusion: Rotational and translational diffusion of an embedded chromophore. *Langmuir* **2007**, *23*, 11677– 11683.
- LARSEN, K.E.; SCHMITZ, Y.; TROYER, M.D.; MOSHAROV, E.; DIETRICH, P.; QUAZI, A.Z.; SAVALLE, M.; NEMANI, V.; CHAUDHRY, F.A.; EDWARDS, R.H.; *et al.* α-Synuclein overexpression in PC12 and chromaffin cells impairs catecholamine release by interfering with a late step in exocytosis. *JNeurosci* **2006**, *26*, 11915–11922.
- LASHUEL, H.A.; PETRE, B.M.; WALL, J.; SIMON, M.; NOWAK, R.J.; WALZ, T.; LANSBURY, P.T. JR. α- Synuclein, especially the Parkinson's disease-associated mutants, forms pore-like annular and tubular protofibrils. *J Mol Biol* **2002**, *322*, 1089–1102.
- LAVEDAN, C. The synuclein family. *Genome Res* **1998**, *2*, 871–880.
- LOWTHER, T.W.; WHANG, Y.; SAMPSON, P.B.; HONEK, J.F.; MATTHEWS, B.W. Insights into the mchanism of *E.coli* methionine aminopeptidase from the structural analysis of reaction products and phosphorous-based transition state analogs. *Biochemistry* **1999**, *38*, 14810-14819.
- LUCKE, C.; GANTZ, D.L.; KLIMTCHUK, E.; HAMILTON, J.A. Interactions between fatty acids and α-synuclein. *J Lipid Res* **2006**, *47*, 1714–1724.
- MADINE, J.; HUGHES, E.; DOIG, A.J.; MIDDLETON, D.A. The effects of alpha-synuclein on phospholipid vesicle integrity: a study using 31P NMR and electron microscopy. Mol. Membr. Biol **2008**, *25*, 518–527.
- MALTSEV, A.S.; CHEN, J.; LEVINE, R.L.; BAX, A. Site-specific interaction between α-synuclein and membranes probed by NMR-observed methionine oxidation rates. *J Am Chem Soc* **2013**, *27135(8),* 2943-6.
- MARTÍNEZ-RUMAYOR, A.; ARRIETA, O.; SOTELO, J.; GARCÍA, E. *Female gender but not cigarette smoking delays the onset of Parkinson's disease.* Clin. Neurol. Neurosurg., 2009.
- MIDDLETON, E.R.; RHOADES, E. Effects of Curvature and Composition on α-Synuclein Binding to Lipid Vesicles. *Biophysical Journal* **2010**, *99*, *7*, 2279-2288.
- MIKKELSEN, S.R.; CORTON E. *Bioanalytical Chemistry*, *68*, no.6; Hoboken: American Chemical Society, 2004.

- MILLER, I.N.; CRONIN-GOLOMB, A. *Gender differences in Parkinson's disease: clinical characteristics and cognition*. Mov. Disor., 2010.
- MORI, S.; HOWARD, G. B. *Size Exclusion Chromatography*; Springer Science & Business Media, 1999.
- MULGREW-NESBITT, A.; DIRAVIYAM, K.; WANG, J.; SINGH, S.; MURRAY, P.; LI, Z.; ROGERS, L.; MIRKOVIC, N.; MURRAY, D. The role of electrostatics in protein-membrane interactions. *Biochim. Biophys. Acta - Mol. Cell Biol. Lipids* **2006**, *1761*, 812–826.
- NARHI, L.; WOOD, S.J.; STEAVENSON, S.; JIANG, Y.; WU, G.M.; ANAFI, D.; KAUFMAN, S.A.; MARTIN, F.; SITNEY, K.; DENIS, P.; *et al*. Both familial Parkinson's disease mutations accelerate α-synuclein aggregation. *J Biol Chem* **1999**, *274*, 9843–9846.
- NOWAKOWSKI, A. B.; WOBIG, W. J.; PETERING, D. H. Native SDS-PAGE: high resolution electrophoretic separation of proteins with retention of native properties including bound metal ions. *Met.* **2014**, *6*, 1068–1078.
- OBESO, J.A.; STAMELOU, M.; STOESSL, A.J. *Past, present, and future of Parkinson's disease: A special essay on the 200th Anniversary of the Shaking Palsy.* Mov. Disor, 2017.
- OLANOW, C.W.; TATTON, W.G. *Etiology and pathogenesis of Parkinson's disease*. Annu. Rev. Neurosci., 1999.
- OSTREROVA, N.; PETRUCELLI, L.; FARRER, M.; MEHTA, N.; CHOI, P.; HARDY, J.; WOLOZIN, B. α- Synuclein shares physical and functional homology with 14-3-3 proteins. *J Neurosci* **1999**, *19*, 5782–5791.
- PALEOLOGOU, K.E. *Phosphorylation at Ser-129 but not the phosphomimics S129E/D inhibits the fibrillation of alpha-synuclein*. J Biol Chem, 2008.
- PECORA, R. *Dynamic Light Scattering: Applications of Photon Correlation Spectroscopy*, Plenum Press, 1985.
- PENNINGTON, S.; SNELL, K.; LEE, M. *The cause of death in idiopathic Parkinson's disease.* Parkinsonism Relat. Disord., 2010.
- PFEFFERKORN, C.M.; HEINRICH, F.; SODT, A.J.; MALTSEV, A.S.; PASTOR, R.W.; LEE, J.C. Depth of α-synuclein in a bilayer determined by fluorescence, neutron reflectometry, and computation. *Biophys J* **2012**, *102*, 613-621.
- RAJAGOPALAN, S.; ANDERSEN, J.K. Alpha synuclein aggregation: is it the toxic gain of function responsible for neurodegeneration in Parkinson's disease? *Mechanisms of Ageing and Development* **2001**, *122*, 1499-1510.
- RAMEZANI, M.; WILKES, M.M.; DAS, T.; HOLOWKA, D.; ELIEZER, D.; BAIRD, B. Regulation of exocytosis and mitochondrial relocalization by alpha-synuclein in a mammalian cell model. *BioRxiv* **2018** *492066*.
- ROCHET, J.C.; CONWAY, K.A.; LANSBURY, P.T. JR. Inhibition of fibrillization and accumulation of prefibrillar oligomers in mixtures of human and mouse α-synuclein. *Biochemistry* **2000**, *39*: 10619–10626.
- RODGER, A. *Circular dichroism and linear dichroism*. Oxford University Press, 1997.
- RODRIGUEZ, J.; IVANOVA, M.; SAWAYA, M.; *et al.* Structure of the toxic core of α-synuclein from invisible crystals. *Nature* **2015***, 525***,** 486–490.
- SAAD, T.; SEEMAN, Q. *Size Exclusion Chromatography and Size Exclusion HPLC of Proteins,* ISLAM Interdisciplinary Biotechnology Unit Aligarh Muslim University Aligarh, UP; India, 2002
- SCOTT, D.; ROY, S. α-Synuclein inhibits intersynaptic vesicle mobility and maintains recycling-pool homeostasis. *J Neurosci* **2012**, *32*, 10129–10135.
- SEGREST, J.P.; DE LOOF, H.; DOHLMAN, J.G.; BROUILLETTE, C.G.; ANANTHARAMAIAH, G.M. Amphipathic helix motif: classes and properties. *Proteins* **1990**, *8*, 103–117.

- SEGREST, J.P.; JACKSON, R.L.; MORRISETT, J.D.; GOTTO, A.M. A molecular theory of lipidprotein interactions in the plasma lipoproteins. *FEBS Lett* **1974**, *38*, 247–253.
- SHAHEEN, S.M.; SHAKIL AHMED, F.R.; HOSSEN, M.N.; AHMED, M.; AMRAN, M.S.; UL-ISLAM, M.A. Liposome as a carrier for advanced drug delivery. *Pak J Biol Sci* **2006**, *9(6)*, 1181– 1191.
- SHOEMAKER, B.A.; PORTMAN, J.J.; WOLYNES, P.G. Speeding molecular recognition by using the folding funnel: The fly-casting mechanism. *Proc. Natl. Acad. Sci*. **2000**, *97*, 8868–8873.
- SOPER, J.H.; KEHM, V.; BURD, C.G.; BANKAITIS, V.A.; LEE, V.M. Aggregation of α- synuclein in S. cerevisiae is associated with defects in endosomal trafficking and phospholipid biosynthesis. *J Mol Neurosci* **2011**, *43*, 391–405.
- SORENSEN, C.S.; KJAERGAARD, M. Effective concentrations enforced by intrinsically disordered linkers are governed by polymer physics. *Proc Natl Acad Sci* **2019**, *116*, 23124-23131.
- SOUZA, J.M.; GIASSON, B.I.; CHEN, Q.; LEE, V.M.; ISCHIROPOULOS, H. Dityrosine crosslinking promotes formation of stable α-synuclein polymers. Implication of nitrative and oxidative stress in the pathogenesis of neurodegenerative synucleinopathies. *J Biol Chem* **2000**, *275*, 18344– 18349.
- SPILLANTINI, M.G.; CROWTHER, R.A.; JAKES, R.; HASEGAWA, M.; GOEDERT, M. Alpha-Synuclein in filamentous inclusions of Lewy bodies from Parkinson's disease and dementia with Lewy bodies. *Proc Natl Acad Sci U S A* **1998**, *95*, 6469–6473.
- SPILLANTINI, M.G.; SCHMIDT, M.L.; LEE, V.M.; TROJANOWSKI, J.Q.; JAKES, R.; et al. Alpha- synuclein in Lewy bodies. *Nature* **1997**, *388*, 839–840.
- STAFFORD, G. C. J.; KELLEY, P. E.; SYKA, J. E. P.; REYNOLDS, W. E.; TODD, J. F. J. Recent improvements in and analytical applications of advanced ion trap technology. *Int. J. Mass Spectrom. Ion Processes* **1984,** *60*, 85–98.
- STANLEY, C.; PETER, H. Calculation of protein extinction coefficients from amino acid sequence data. *Analytical Biochemistry* **1989**, *182*, 2, 319-326.
- STEPHEN, K.; VAN DEN EEDEN; CAROLINE, M.; TANNER; ALLAN, L.; BERNSTEIN; ROBIN, D.; FROSS; LEIMPETER, A.; DANIEL, A.; BLOCH; LORENE, M.; NELSON. Incidence of Parkinson's Disease: Variation by Age, Gender, and Race/Ethnicity. *Am. J. Epidemiol*. **2003**, *157, 1015–1022*.
- STETEFELD, J.; MCKENNA, S.A.; PATEL, T.R. Dynamic light scattering: a practical guide and applications in biomedical sciences. *Biophys Rev* **2016**, *8*, 409–427.
- TABOR, S.; RICHARDSON, C.C. *A bacteriophage T7 RNA polymerase/promoter system for controlled exclusive expression of specific genes*. Proc Natl Acad Sci USA, 1985.
- TAHIROV, T.H.; OKI, H.; TSUKIHARA, T.; OGASAHARA, K.; YUTANI, K.; OGATA, K.; IZU, Y.; TSUNASAWA, S.; KATO, I. Crystal structure of methionine aminopeptidase from hyperthermophile, Pyrococcus furiosus. *J Mol Biol*. **1998**, *284(1),* 101-24.
- THAYANIDHI, N.; HELM, J.R.; NYCZ, D.C.; BENTLEY, M.; LIANG, Y.; HAY, J.C. α-Synuclein delays endoplasmic reticulum (ER)-to-Golgi transport in mammalian cells by antagonizing ER/Golgi SNAREs. *Mol Biol Cell* **2010**, *21*, 1850–1863.
- ULMER, T.S.; BAX, A.; COLE, N.B.; NUSSBAUM, R.L. Structure and dynamics of micelle- bound human α-synuclein. *J Biol Chem* **2005**, *280*, 9595–9603.
- UVERSKY, V.N. Neuropathology, biochemistry, and biophysics of α-synuclein aggregation. *J Neurochem* **2007**, *103*, 17–37.
- UVERSKY, V.N.; YAMIN, G.; SOUILLAC, P.O.; GOERS, J.; GLASER, C.B.; FINK, A.L. Methionine oxidation inhibits fibrillation of human alpha-synuclein in vitro. *FEBS Lett* **2002**, *517(1-3)*, 239-44.

- VAN DER SCHYF, C.J. *The use of multi-target drugs in the treatment of neurodenegerative di- seases.* Expert Rev. Clin. Pharmacol., 2011.
- VARKEY, J.; ISAS, J.M.; MIZUNO, N.; JENSEN, M.B.; BHATIA, V.K.; JAO, C.C.; PETRLOVA J.; VOSS, J.C.; STAMOU, D.G.; STEVEN, A.C.; et al. Membrane curvature induction and tubulation are common features of synucleins and apolipoproteins. *J Biol Chem* **2010**, *285*, 32486–32493.
- WANG, L.; DAS, U.; SCOTT, D.A.; TANG, Y.; MCLEAN, P.J.; ROY, S. α-Synuclein multimers cluster synaptic vesicles and attenuate recycling. *Curr Biol* **2014**, *24*, 2319–2326.
- WEI, Y.; THYPARAMBIL, A.A.; ROBERT, A.L. Protein Helical Structure Determination Using CD Spectroscopy for Solutions with Strong Background Absorbance from 190-230 nm. *Biochimica et biophysica acta*. **2014**, *1844(12).*
- WU, B.; LIU, Q.; DUAN, C.; LI, Y.; YU, S.; CHAN, P.; UEDA, K.; YANG, H. Phosphorylation of α-synuclein upregulates tyrosine hydroxylase activity in MN9D cells. *Acta Histochem* **2011**, *113*, 32–35.
- YONETANI, M.; NONAKA, T.; MASUDA, M.; INUKAI, Y.; OIKAWA, T.; HISANAGA, S.; HASEGAWA, M. Conversion of wildtype α-synuclein into mutant-type fibrils and its propagation in the presence of A30P mutant. *J Biol Chem* **2009**, *284*, 7940–7950.
- YU, S.; ZUO, X.; LI, Y.; ZHANG, C.; ZHOU, M.; ZHANG, Y.A.; UEDA, K.; CHAN, P. Inhibition of tyrosine hydroxylase expression in α-synuclein-transfected dopaminergic neuronal cells. *Neurosci Lett* **2004**, *367*, 34–39.
- YU, Y.Q.; GILAR, M.; LEE, P.J.; BOUVIER, E.S.; GEBLER, J.C. Enzyme-friendly, mass spectrometry-compatible surfactant for in-solution enzymatic digestion of proteins. *Anal Chem* **2003**, *75(21),* 6023-8.
- YUAN, H. Treatment strategies for Parkinson's disease. *Neurosci. Bull.* **2010**, *26*, 66-76.
- ZHANG, Y.; LARCHER, K.M.; MISIC, B.; DAGHER, A. *Anatomical and functional organization of the human substantia nigra and its connections.* eLife, 2017.
- ZHU, M.; FINK, A.L. Lipid binding inhibits α-synuclein fibril formation. *J. Biol. Chem*, **2003**, *278*, 16873–16877.
- ZIMMERBERG, J.; KOZLOV, M.M. How proteins produce cellular membrane curvature. *Nat. Rev. Mol. Cell Biol* **2006**, *7*, 9–19.